Journal of Inorganic Biochemistry 194 (2019) 97–113

Contents lists available at ScienceDirect

Journal of Inorganic Biochemistry

journal homepage: www.elsevier.com/locate/jinorgbio

Redox-cycling and intercalating properties of novel mixed copper(II) complexes with non-steroidal anti-inflammatory drugs tolfenamic, mefenamic and flufenamic acids and phenanthroline functionality: Structure, SOD-mimetic activity, interaction with albumin, DNA damage study and anticancer activity

Miriama Simunkova[a], Peter Lauro[b], Klaudia Jomova[b], Lenka Hudecova[b], Martin Danko[c], Saleh Alwasel[d], Ibrahim M. Alhazza[d], Simona Rajcaniova[e], Zuzana Kozovska[e], Lucia Kucerova[e], Jan Moncol[f], Lubomir Svorc[g], Marian Valko[a,d,*]

[a] Department of Physical Chemistry, Faculty of Chemical and Food Technology, Slovak University of Technology, 812 37 Bratislava, Slovakia
[b] Department of Chemistry, Faculty of Natural Sciences, Constantine the Philosopher University, 949 74 Nitra, Slovakia
[c] Polymer Institute SAS, Dubravska cesta 9, 845 41 Bratislava, Slovakia
[d] College of Science, King Saud University, Saudi Arabia
[e] Laboratory of Molecular Oncology, Cancer Research Institute of Biomedical Research Centre SAS, Dubravska cesta 9, 845 05 Bratislava, Slovakia
[f] Department of Inorganic Chemistry, Faculty of Chemical and Food Technology, Slovak University of Technology, 812 37 Bratislava, Slovakia
[g] Institute of Analytical Chemistry, Faculty of Chemical and Food Technology, Slovak University of Technology, 812 37 Bratislava, Slovakia

ARTICLE INFO

Keywords:
Cu complexes
NSAID, Phenanthroline
Intercalation
SOD activity
Anticancer activity

ABSTRACT

Copper(II) complexes containing non-steroidal anti-inflammatory drugs (NSAIDs) have been the subject of many research papers and reviews. Here we report the synthesis, spectroscopic study and biological activity of novel mixed copper(II) complexes with NSAIDs: tolfenamic (tolf), mefenamic (mef) and flufenamic (fluf) acids and phenanthroline (phen): [Cu(tolf-*O*,*O*′)$_2$(phen)] (**1**), [Cu(mef-*O*,*O*′)$_2$(phen)] (**2**), [Cu(fluf-*O*,*O*′)$_2$(phen)] (**3**). Complexes were characterized by X-ray analysis and EPR spectroscopy. Complexes **1–3** are monomeric, six-coordinate and crystallize in a monoclinic space group. Interaction of Cu(II) complexes with DNA was studied by means of absorption titrations, viscosity measurements and gel electrophoresis. The relative ability of the complexes to cleave DNA even in the absence of hydrogen peroxide is in the order **3** > **2** > **1**. Application of the reactive oxygen species (ROS) scavengers, L-histidine, DMSO and SOD confirmed that singlet oxygen, hydroxyl radicals (Fenton reaction) and superoxide radical were formed, respectively. Thus, in addition to mechanism of intercalation, redox-cycling mechanism which in turn lead to the formation of ROS contribute to DNA damage. Cu(II) complexes exhibit excellent SOD-mimetic activity in the order **3**~**1** > **2**. The fluorescence spectroscopy revealed that albumin may act as a targeted drug delivery vehicle for Cu(II) complexes (K~10^6). The anticancer activities of complexes **1–3** were investigated using an MTS assay (reduction of the tetrazolium compound) against three cancer cell lines (HT-29 human colon adenocarcinoma, HeLa and T-47D breast cancer cells) and mesenchymal stromal cells (MSC). The most promising compound, from the viewpoint of its NSAID biological activity is **3**, due to the presence of the three fluorine atoms participating in the formation of weak hydrogen-bonds at the DNA surface.

1. Introduction

With the aim to develop a new class of metal-based anticancer drugs, attention has been paid to the design of metal complexes with multiple modes of action and a higher efficacy, as compared with cisplatin derivatives [1–5]. One of the mechanisms of action of the anticancer drugs is intercalation. A promising class of anticancer drugs that serve this purpose are metallo-intercalators. They contain planar

* Corresponding author at: Department of Physical Chemistry, Faculty of Chemical and Food Technology, Slovak University of Technology, 812 37 Bratislava, Slovakia.
E-mail address: marian.valko@stuba.sk (M. Valko).

https://doi.org/10.1016/j.jinorgbio.2019.02.010
Received 27 December 2018; Received in revised form 15 February 2019; Accepted 18 February 2019
Available online 23 February 2019
0162-0134/

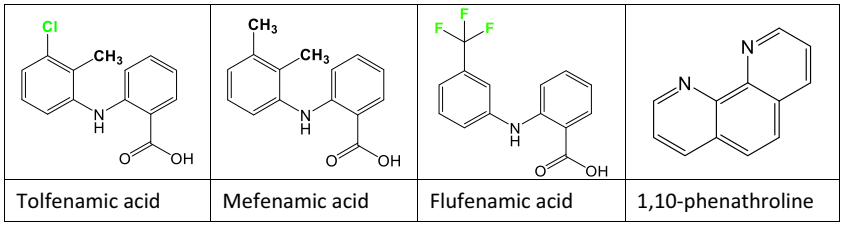

Fig. 1. Structures of tolfenamic (tolf), mefenamic (mef) and flufenamic (fluf) acids and 1,10-phenanthroline (phen).

aromatic rings that can undergo non-covalent interactions with the DNA molecule, as a result of π-π stacking and dipole-dipole interactions [6,7]. The interaction of metal-based drugs with DNA results in an unwinding and extension of DNA in order to accommodate the metal-complexes between the base pairs [8–11].

The redox metabolism of cancer cells is different from that of healthy cells and is characterized by the formation of increased concentrations of intracellular reactive oxygen species (ROS) [12]. Further enhancement of ROS levels and/or inhibition of ROS detoxifying enzymes (e.g. glutathione) in cancer cells appears to occur as an anticancer mechanism of metal-based drugs, in addition to intercalation. Indeed, redox cycling involving metal-based drugs is considered to be the key mechanism for an increased formation of ROS, which in turn may cause cancer cell death, as a result of DNA damage [12–14].

Due to its bioavailability, copper has a rich and varied history in medicinal chemistry, in the form of compounds used as antibacterial and anticancer agents [15–17]. There is considerable interest in using copper in place of platinum in therapeutic agents, because it is much better tolerated, mainly as a result of natural biological pathways which regulate Cu levels [15]. The variability in the structural chemistry of copper complexes has been termed a “plasticity effect” [18]. This feature, which is typical for Cu(II) complexes, has been associated with oxygen-dependent or oxygen-independent DNA cleavage of cancer cells. Indeed, numerous Cu(II) complexes are potentially effective as anticancer, anti-inflammatory, and antimicrobial agents, in addition to functioning as chemical nucleases.

Of particular interest are copper complexes containing coordinated non-steroidal anti-inflammatory drugs (NSAIDs), which exhibit redox-cycling properties, improved anti-inflammatory activity and suppressed gastrointestinal toxicity, as compared with the free, uncomplexed drug [19]. In addition, copper complexes with NSAID have been shown to have potent antiulcerogenic and antiviral activities. A series of excellent comprehensive papers on copper complexes with a variety of NSAIDs has been published by Psomas and his coworkers [20–25].

Inflammation is the primary response of the immune system to infection; however, chronic inflammation has been found to be responsible for various pathological states of an organism, including arthritis, cancer, cardiovascular disease, neurodegenerative disorders and stroke [26]. The process of inflammation is accompanied by the formation of reactive, pro-inflammatory superoxide radical anions, which are produced by nicotinamide adenine dinucleotide phosphate (NAD(P)H) oxidases and may in turn lead to toxic effects on an organism. Copper complexes containing NSAIDs are known to be effective scavengers of superoxide radical anions (superoxide dismutase (SOD)-mimetics) and anti-inflammatory agents with a lower toxicity and reduced side effects than the uncoordinated NSAID drugs [19,27]. The beneficial effect of copper complexes containing NSAIDs, in suppressing the inflammatory response, is due to redox cycling between cupric (Cu^{2+}) and cuprous (Cu^{+}) oxidation states with the concomitant oxidation of superoxide radical anions to form molecular oxygen ($Cu^{2+} + O_2\cdot^- \rightarrow Cu^{+} + O_2$). In the process of redox-cycling, additional ROS such as hydroxyl radicals, may be formed which can act as effective agents for DNA cleavage. Thus, the process of redox cycling may convert a relatively unreactive superoxide radical anion to more reactive ROS which may cause DNA-damage. Hence, the suppressed SOD activity found in various cancer cells can be compensated for by copper-NSAID complexes, which act as an effective substitute for SOD, and result in an efficient transformation of superoxide radicals to more reactive ROS. The penetration of Cu-NSAID complexes through cell membranes is facilitated by their relatively low molecular mass and reasonable solubility in lipids.

1,10-Phenanthroline, which possesses intercalating properties, is another functionality, which when coordinated to copper, has nuclease activity and can induce DNA strand breakage [28]. In addition, it was demonstrated that also hydrogen peroxide is involved in the mechanism of the DNA damage by copper-phenanthroline complexes, which substantiates the involvement of hydroxyl radicals in the process.

In the present work, we combined properties of both, ROS-mediating and intercalating functionalities for the design of novel anticancer Cu(II) complexes with non-steroidal anti-inflammatory drugs - tolfenamic (tolf), mefenamic (mef) and flufenamic (fluf) acids and the intercalating ligand phenanthroline (phen) (Fig. 1). These three NSAIDs differ in the choice of substituents on the benzene ring. Flufenamic and tolfenamic acids contain fluorine and chlorine atoms, respectively, while mefenamic acid contains methyl groups. We propose that the structural differences represented by either halogenation or methylation of the benzene rings in the NSAIDs may affect both the intercalation ability, and the redox-cycling properties of the Cu(II) complexes. These structural differences are later considered in detail, from the point of view of their DNA damaging potential via ROS-induced damage, and by the efficiency of their intercalation into DNA. The determination of DNA damage by the copper complexes was made in more detail by screening their anticancer activity against several different cancer cell lines and mesenchymal cells. To correlate molecular structure vs biological activity, the complexes were characterized by X-ray analysis and spectroscopic methods. Binding affinity studies of Cu(II) complexes to human serum albumin were also performed.

2. Experimental section

2.1. Chemicals

Copper(II) acetate monohydrate, copper chloride dihydrate, phenanthroline monohydrate, mefenamic acid, flufenamic acid, neocuproine and 18-crown-6 ether were purchased from Sigma-Aldrich. Tolfenamic acid was purchased from TCI. Solvents were obtained from Merck, Serva, Mikrochem and Centralchem. All the chemicals were of analytical grade and were used without further purification. Dimethyl sulfoxide (DMSO) was obtained from Fluka. All the buffer solutions used in the DNA experiments were prepared using purified water (Simplicity Ultrapure Water System, Millipore, Bedford, MA, USA).

All reagents and solvents for the biochemical experiments were of analytical reagent grade and used as supplied. All solutions were prepared using purified water (Simplicity Ultrapure Water System, Millipore, Bedford, MA, USA). The disodium salt of calf thymus DNA, NaH_2PO_4, Na_2HPO_4, hydrogen peroxide (30% solution in water), Xanthine, and Xanthine Oxidase were purchased from Sigma Aldrich (Germany), absolute ethanol, tris(hydroxymethyl)aminomethane (TRIS) base, ampicilin, agarose, ethidium bromide were from Serva (Germany). The glycerol was obtained from Merck (Germany), the 10xTBE (Tris –Borate-EDTA) and bromphenol blue from Applichem (Germany). NBT (Nitro Blue Tetrazolium) was obtained from Duchefa

Biochimie (The Netherlands).

A concentrated stock solution of DNA was prepared by dissolution of the lyophilized sodium deoxyribonucleic acid sodium salt from calf thymus (CT-DNA) salt in a buffer solution containing 5 mM TRIS, 50 mM NaCl at *p*H 7.2 (TBS, Tris Buffer Saline) followed by stirring for three days. The concentration of DNA was determined from its UV absorbance at 260 nm, as measured after being diluted by a factor of 1:100 (NanoDrop ND-1000 spectrophotometer, USA). The solution of CT DNA gave a ratio of UV–Vis absorbances at 260 and 280 nm (A_{260}/A_{280}) in the range of 1.8–1.9, indicating that the DNA was sufficiently protein free [29] and no further purification was necessary. The CT DNA stock solution was kept at 4 °C and used within four days.

2.2. Synthesis

[**Cu(tolf-*O*,*O*′)$_2$(phen)**] (**1**). Copper(II) acetate (0.200 g) was dissolved in methanol to form a 0.02 M solution. To 50 ml of this solution was added 0.198 g of phenanthroline monohydrate. This caused the original copper acetate solution to change in color from turquoise to deep blue. The solution was stirred for 10 min and then 0.523 g of solid tolfenamic acid was added so that the ratio of phenanthroline:tolfenamic acid was 1:2. The resulting olive-colored mixture was stirred for a further 24 h, by when a precipitate was formed, which was filtered off and air-dried for one month. Crystals were obtained by slow evaporation of the solvent. Dark green crystals, suitable for X-ray structure determination, were collected after a further two weeks. Anal. Cal. for $C_{40}H_{30}Cl_2CuN_4O_4$ (MW = 765.25): C, 62.78; H, 3.95; N, 7.32; found: 62.90; H, 3.91; N, 7.35.

[**Cu(mef-*O*,*O*′)$_2$(phen)**] (**2**). Copper(II) acetate (0.200 g) was dissolved in methanol to form a 0.02 M solution. To 50 ml of this solution was added 0.198 g of phenanthroline monohydrate, to give a dark turquoise solution which was stirred for 10 min. Then, the 0.483 g of solid mefenamic acid was added to obtain a ratio of phenanthroline:mefenamic acid = 1:2. The resulting mixture was stirred for 24 h which caused the color to change to olive green. The precipitate was filtered off and air-dried for one month. Dark olive-green crystals suitable for X-ray structure determination were obtained by slow evaporation of the solvent over two weeks. Anal. Cal. for $C_{42}H_{36}CuN_4O_4$ (MW = 724.29): C, 69.65; H, 5.00; N, 7.77; found: C, 69.66; H, 4.94; N, 7.81.

[**Cu(fluf-*O*,*O*′)$_2$(phen)**] (**3**). The copper complex containing flufenamic acid was prepared in an identical manner as for the previous two complexes. Addition of 0.198 g of phenanthroline monohydrate to 50 ml of a 0.02 M methanolic solution of copper(II) acetate caused the mixture to change in color from its original green turquoise to sapphire blue. After stirring for 10 min, 0.562 g of solid flufenamic acid was added to a final ratio of phenanthroline:flufenamic acid = 1:2 and stirred for a further 24 h. The resulting precipitate was filtered off and air-dried. Dark green crystals suitable for X-ray structure determination were obtained after two weeks by slow evaporation of the solvent. Anal. Cal. for $C_{40}H_{26}CuF_6N_4O_4$ (MW = 804.19): C, 59.74; H, 3.26; N, 6.97; found: C, 59.61; H, 3.31; N, 6.91.

2.3. Physical measurements

2.3.1. X-ray crystallography and Hirshfeld surface analysis

Data collection and cell refinement of monocrystals **1–3** were carried out using a Stoe StadiVari diffractometer with a Pilatus3R 300 K detector and microfocus source Xenocs Genix3D Cu HF with CuKα. The structures were solved by direct methods using SIR11 [30] or by a charge-flipping method using SUPERFLIP [31] and were refined using the full-matrix least-squares procedure with SHELXL version 2018/3 [32]. Geometrical analyses were performed with SHELXL. The structures were drawn using the OLEX2 package [33] and MERCURY version 3.10 [34]. The crystal structure of **1** shows disordered tolfenamate anionic ligands in three statistical positions with occupancy factors 0.426(3), 0.310(2) and 0.264(3). The disordered tolfenamate anions of **1** have been modeled using SADI, RIGU, EADP and SUMP instructions in SHELXL. CIF files can be found in the Supplementary Data appendix.

Elemental analysis was carried out using FLASH EA 1112 Series CHN element analyzer. CrystalExplorer [35] was used to calculate Hirschfeld surfaces [36,37] and associated fingerprint plots [38,39]. The Hirshfeld surfaces have been calculated only for major and medium positions of the disordered tolfenamate anion of **1**.

2.3.2. EPR spectroscopy and electronic spectroscopy

EPR spectra were measured at room temperature (290 K) and at 77 K (liquid nitrogen) using a Bruker EMX spectrometer (operating at X band, with 100-kHz field modulation) which was interfaced to a PC for data acquisition. The temperature dependent EPR spectra were measured using a Bruker variable temperature unit. The *g* factors were quoted with an uncertainty of (0.0001) using an internal reference standard marker containing 1,1-diphenyl-2-picrylhydrazyl (DPPH), built into the EPR spectrometer. The simulations of the EPR spectra were performed using the commercially available program SimFonia (Bruker).

The electronic spectra (190–1100 nm) of the copper complexes were recorded at ambient temperature, from their suspensions in Nujol, using a SPECORD 250 Plus (Analytic Jena, Germany) spectrophotometer. The UV–Vis absorption spectra for biochemical experiments were recorded on a Specord 50 PLUS spectrophotometer (Analytic Jena, Germany).

2.3.3. Electrochemical measurements

The electrochemical experiments were made using an Autolab PGSTAT 101 (Metrohm Autolab B.V., The Netherlands) apparatus, in conjunction with the NOVA software (version 1.9). The entire three-electrode system (purchased from DropSens, Asturias, Spain), maintained on a ceramic substrate, consisted of the miniaturized thick-film boron-doped diamond (BDD) working electrode (commercially marked as CBDD110, with the diameter of 3.6 mm and declared boron doping level of 2500 ppm), screen-printed carbon auxiliary electrode and a silver pseudoreference electrode. Cyclic voltammetry (CV) was applied over a potential window ranging from −1.0 to +1.5 V, with a fixed scan rate value of 100 mV/s, by undergoing three scans. The complexes studied were dissolved individually in 10 ml of DMSO and subsequently diluted with 0.1 M NaCl (supporting electrolyte) to a concentration of 1 mM (stock solution). Working solutions of the complexes were prepared by a tenfold dilution of the stock solutions with 0.1 M NaCl. The measurement cell always contained 10 ml of the complex solution. Prior to making the measurement, the particular solution to be studied was degassed by bubbling with N_2 for 10 min to provide an inert environment inside the cell.

2.4. DNA interaction studies

The interaction of copper(II) complexes **1–3** with DNA was studied using absorption titrations and viscometric measurements.

2.4.1. Absorption titrations

Absorption titrations were performed using a constant concentration of the complexes (20 μM) but increasing the concentration of DNA (0–60 μM in TBS buffer, pH 7.2). The sample was allowed to stand for 10 min at room temperature before each spectrum was recorded. Control measurements were carried out for all concentrations of DNA used, in the absence of any complexes and making a correction of the absorbance of the DNA alone. The absorption titration data were used to calculate the intrinsic binding constant (K_b) for each complex, by means of the Wolfe-Shimmer equation [40,41]:

$$\frac{[DNA]}{(\varepsilon_a - \varepsilon_f)} = \frac{[DNA]}{(\varepsilon_b - \varepsilon_f)} + \frac{1}{K_b(\varepsilon_b - \varepsilon_f)} \quad (1)$$

where [DNA] is the concentration of CT DNA in base pairs, ε_a is the apparent extinction coefficient obtained by calculation Aobs/[complex], ε_b refers to the extinction coefficient of the complex in the fully bound form and ε_f corresponds to the extinction coefficient of the complex in its free form. The K_b (M^{-1}) can be calculated by the ratio of slope to the intercept in plots [DNA]/(ε_a-ε_f) versus [DNA].

2.4.2. Viscometric study

Viscometric studies were carried out using the Viscometer S10 at a constant temperature at 25 ± 0.1 °C. CT-DNA solution was prepared at 1 mM in TBS buffer (5 mM TRIS, 50 mM NaCl, pH 7.2). A stock solution of each complex (**1**, **2**, **3**) and ethidium bromide, all prepared at a concentration of 4 mM in DMSO, was added according to increasing [compound]/[DNA] ratios of 0.02, 0.04, 0.06, 0.08, and 0.1, and the viscosity was measured for each one. Triplicate measurements were made for each sample, and an average viscosity was calculated. The data were presented as the relative solution viscosity $(\eta/\eta_0)^{1/3}$ versus [compound]/[DNA] ratio, where η and η_0 are the viscosities of DNA in the presence and absence of compound, respectively.

2.5. Nuclease-like activities of copper(II) complexes

2.5.1. Purification of plasmid DNA

An *E. coli* DH5α (engineered *E. coli* cells in order to maximize transformation efficiency) cell culture containing plasmid DNA pBSK+ was grown in LB/Amp medium for 16 h at 37 °C under continual shaking at 150 rpm (Heidolf Unimya 1010, Germany). Plasmid DNA (pDNA) was isolated using a Fast-n-easy Plasmid Mini-Prep Kit (Jena Bioscience) following the instructions in the isolation protocol. The concentration of DNA was measured using a NanoDrop ND–1000 spectrophotometer (Nanodrop Technologies, USA). Absorbance ratios A_{260}/A_{230} in the range 2.0–2.2 and $A_{260}/A_{280} \geq 1.8$, determined for all DNA samples used, indicated a sufficient purity in all cases.

2.5.2. DNA cleavage experiments

The ability of the complexes to cleave DNA was studied by agarose gel electrophoresis. The reaction mixture contained 15 μM of pBSK+ DNA in 50 mM sodium phosphate buffer (*p*H 7.4) and the solution of the copper complex in DMSO at final concentrations of 5, 10, 25, 40, 50 μM, in a 15 μl volume. Experiments were performed both in the absence and presence of hydrogen peroxide (50 μM H_2O_2). Samples were incubated for 1 h at 37 °C. The reactions were quenched by adding a loading buffer (4 μl) containing 0.25% bromophenol blue in 30% glycerol. The samples were loaded directly onto 0.8% agarose gel in TBE (Tris-borate-EDTA) containing 89 mM Tris-borate acid and 2 mM EDTA at *p*H = 8.0 and electrophoresed at 80 V in a 1xTBE buffer. The 1 kb DNA ladder (Jena Bioscience) was used as a standard. A reference plasmid sample was linearized with *Eco*RI endonuclease (Fast digest EcoRI, Fermentas) and used as a control for double strand breaks. A gel was stained with 0.5 μg/ml of ethidium bromide and photographed under UV light (Kodak Gel Logic 200, Eastman Kodak Company, USA). Mechanisms of DNA cleavage were evaluated by the addition of radical scavenging agents, e.g. L-Histidine (for singlet oxygen, $^1O_2$), DMSO (for hydroxyl radicals, ·OH), and superoxide dismutase enzyme (for superoxide radical anion, $O_2\cdot^-$). The radical scavenging agents were added to each pDNA sample prior to the addition of the complex.

2.6. SOD-mimetic activity of copper(II) complexes

The ability of the copper complexes to scavenge the superoxide radical anions was determined using the NBT (tetrazolium blue, Nitro-Blue-Tetrazolium) test in which the xanthine/xanthine oxidase (X/XO) system was used for superoxide production [42]. The extent of NBT reduction was monitored spectrophotometrically by measuring the absorbance at 550 nm. The reaction mixture contained 0.2 mM xanthine, 0.6 mM NBT in 0.1 mM sodium phosphate buffer at pH 7.8 and at 25 °C in a volume of 3 ml. The tested compounds were dissolved in DMSO. The measured concentrations of the compounds were as follows: 0.083; 0.166; 0.25; 0.5; 1; 2; 3; 4; 5; 6 μM. The reaction was started by adding xanthine-oxidase (XO) into the reaction mixture at a concentration sufficient to give an absorbance change (ΔA/min) between 0.025 and 0.035. Each experiment was performed in triplicate. The SOD activity of metal-complexes was defined to be the concentration of the tested compound that causes 50% inhibition of NBT reduction by the superoxide radical in the X/XO system (IC_{50} value) [43].

The formation of Cu(I) ions upon reduction with superoxide radical anion was demonstrated by means of UV/Vis spectroscopy using the specific Cu(I) chelating agent neocuproine (2,9-dimethyl-1,10-phenantroline). Potassium dioxide (KO_2) was used as a source of superoxide anion radicals and was stabilized using 18-crown-6 ether. 500 μl of 1 mM DMSO solution of complexes **1–3**, 500 μl of 1 mM potassium dioxide DMSO solution and 500 μl of 0.02 M neocuproine DMSO solution were mixed together, whereupon the absorbance at 458 nm was measured using a Shimadzu UV/Vis-NIR spectrometer.

2.7. Human serum albumin binding studies

Binding of copper(II) complexes **1–3** to human serum albumin (HSA) was studied by tryptophan fluorescence quenching experiments using HSA (2 μM) in sodium phosphate buffer (pH 7.4). Albumin was excited at 295 nm and the fluorescence emission intensity quenching of tryptophan residues due to the binding of complexes **1–3** to HSA was detected at 347 nm (maximum emission). Fluorescence spectra were recorded in the range 300 to 525 nm with an increasing concentration of complexes **1–3** (up to 15 μM) present as quenchers. The Stern–Volmer and Scatchard equations have been used to evaluate the interaction of quenchers with albumin. The Stern-Volmer equation can be expressed in the form [20].

$$I_0/I = 1 + k_q\tau_0[Q] = 1 + K_{SV}[Q] \quad (2)$$

where K_{SV} (M^{-1}) is the value of dynamic quenching constant, k_q ($M^{-1}\,s^{-1}$) is the quenching constant that characterizes the interaction of complexes **1–3** with albumin, τ_0 is the average lifetime of albumin in the absence of quencher and [Q] is the concentration of the quencher. I_0 is the initial fluorescence intensity of tryptophan residues of albumin, and I are the fluorescence intensities of albumin after addition of the quenchers (complexes). The fluorescence lifetime (τ_0) of tryptophan in albumin is about 10^{-8} s [44]. K_{SV} can be obtained from the slope of the I_0/I versus [Q] plot, which in turn allows k_q to be calculated.

The Scatchard equation [45]

$$\frac{\Delta I/I_0}{[Q]} = nK - K\frac{\Delta I}{I_0} \quad (3)$$

allows the calculation of the association binding constant K (M^{-1}) from the slope of the ($\Delta I/I_0$)/[Q] versus $\Delta I/I_0$ plot, and the number of binding sites is obtained from the intercept.

2.8. Anticancer activity of copper(II) complexes

2.8.1. Cell lines

Human colon adenocarcinoma cell lines HT-29 (ATCC® HTB-38™), human cervical cancer cells Hela (ATCC® CCL-2™), human breast cancer cells T-47D (ATCC® HTB-133™), mesenchymal stromal cells (MSC) were obtained from healthy individuals undergoing elective liposaspiration. All participants provided an informed consent. No humans were involved in this research study, human material harvested from the healthy individuals after elective surgery was used as approved by the Ethics Committee of the University Hospital (Ruzinov, Ruzinovska 6, 826 06 Bratislava, Slovakia).

Mesenchymal stromal cells (MSC) were isolated and characterized by the immunophenotype and differentiation potential as previously described in [46]

Cancer cells were cultured in high-glucose (4.5 g/L) and MSC in low glucose (1 g/L) Dulbecco's modified Eagle medium (DMEM, PAN Biotech, Germany), supplemented with 5 or 10% fetal bovine serum (FBS, Biochrom AG), 2 mM glutamine or glutamax and antibiotic-antimycotic mix (GIBCO BRL, Gaithesburg, MD). Cells were maintained at 37 °C in humidified atmosphere and 5% CO_2.

2.8.2. MTS assay

The MTS (3-(4,5-dimethylthiazol-2-yl)-5-(3-carboxymethoxyphenyl)-2-(4-sulfophenyl)-2H-tetrazolium) assay protocol is based on the reduction of the MTS tetrazolium compound by viable mammalian cells (and cells from other species) to generate a colored formazan dye that is soluble in cell culture media. The analysis was performed in 96-well plates (TPP Cat. n. 92,096). Depending on the particular cell line, 4.10^3–5.10^3 cells per well were seeded. After 24 h, cells were exposed to various concentrations of complexes **1–3**. The cytotoxic effect of agents tested on human colon adenocarcinoma cells HT-29, human cervical cancer cells Hela, human breast cancer cells T-47D and mesenchymal stromal cells (MSC) was determined using MTS assay (Promega, G3582). Measurements were performed after 4 days of cultivation. Tests were performed in quadruplicates. The IC_{50} values were calculated using the Calcusyn software.

3. Results and discussion

Copper(II) complexes containing two functionalities, phenanthroline and NSAIDs tolfenamic, mefenamic and flufenamic acids, were prepared, with the aim to study their effectiveness as prospective anticancer agents. Specifically, it was aimed to correlate the molecular structure of the complexes with their ability to intercalate into DNA, to interact with albumin, to scavenge superoxide radical anions, and to kill cancer cells. Initially, we now report the structural characteristics of all three complexes both in the solid state and in solution.

3.1. X-ray structure of Cu(II) complexes

All three copper(II) complexes, [Cu(tolf-*O*,*O*′)$_2$(phen)] (**1**), [Cu(mef-*O*,*O*′)$_2$(phen)] (**2**), [Cu(fluf-*O*,*O*′)$_2$(phen)] (**3**) are monomeric and crystallize in the monoclinic space group *C*2/*c*; however, while complexes **1** and **2** are isostructural, **3** has a slightly different crystal structure, although it is also monomeric. The copper atoms in all mononuclear structures lie in a particular position on two-fold axes, and their coordination environment has a strongly distorted octahedral symmetry. The X-ray crystal data are summarized in Table 1.

The molecular structures of all three complexes are very similar (see Fig. 2), with intercalator (1,10-phenanthroline) and NSAIDs (tolfenamic, mefanamic and flufenamic acids) being coordinated to the Cu atom as bidentate chelating ligands. The copper atoms in all three complexes are chelated in the equatorial plane by two nitrogen atoms, from the 1,10-phenanthroline moiety, and two carboxylate oxygen atoms of two tolfenamate, mefenamate and flufenamate anions. While the equatorial plane of all three compounds (2*N*2*O*) is essentially planar, the axial positions are strongly distorted as a result of the limited bidentate bonding ability of oxygen atoms from carboxylate groups of the NSAIDs. The tolfenamate anion (complex **1**), mefanate anion (complex **2**) and flufenamate anion (complex **3**) are coordinated to the copper atom with equivalent distances of 2.942(13) Å (**1**), 2.7054(13) Å (**2**), 2.5708(14) Å (**3**), respectively. Selected bond distances are given in Table 2.

Interestingly, an X-ray structural analysis of complex **1** revealed that the tolfenamate anions show disorder in three statistical positions (Fig. 3).

The molecular structures of all three complexes are stabilized by intermolecular hydrogen bonds NH···O between the hydrogen atom of an NH- group and an oxygen atom of the carboxylate group from the anionic ligands. The distance of the hydrogen bonding interaction is 2.769 Å, in the case of compound **1**; 2.695 Å, for compound **2**; and 2.688 Å, for compound **3**.

Table 1
X-ray data for [Cu(tolf-*O*,*O*′)$_2$(phen)] (**1**), [Cu(mef-*O*,*O*′)$_2$(phen)] (**2**), [Cu(fluf-*O*,*O*′)$_2$(phen)] (**3**).

Complex	1	2	3
Empirical formula	$C_{40}H_{30}Cl_2CuN_4O_4$	$C_{42}H_{36}CuN_4O_4$	$C_{40}H_{26}CuF_6N_4O_4$
M [g·mol^{-1}]	765.25	724.29	804.19
T [K]	295	100	100
Crystal system	Monoclinic	Monoclinic	Monoclinic
Space group	C2/c	C2/c	C2/c
a [Å]	12.2074(5)	11.8766(4)	12.2373(7)
b [Å]	10.8471(5)	11.5577(2)	10.4404(6)
c [Å]	25.7560(9)	24.3039(8)	26.1573(17)
α [°]	90	90	90
β [°]	90.421(3)	94.581(3)	93.767(5)
γ [°]	90	90	90
V [Å^3]	3410.4(2)	3325.45(17)	3334.7(3)
Z	4	4	4
ρ [g·cm^{-3}]	1.490	1.447	1.602
μ [mm^{-1}]	2.753	1.344	1.667
Goodness-of-fit on F^2	1.063	0.923	1.019
R1	0.0623	0.0328	0.0349
wR_2 [all data]	0.1891	0.0798	0.1020
Largest diff. Peak/hole[e Å^{-3}]	0.28/−0.43	0.46/−0.51	0.35/−0.46
CCDC no.	1,874,405	1,874,407	1,874,406

The molecular packing is also determined by bond and torsion angles, which determine the stereochemical outcomes of the molecular structure: because the stereochemical interactions are different in each compound, the packing of its molecules is also different. Complexes **1** and **2** have very similar molecular packing, because tolfenamic and mefenamic acids are isostructural; however, molecular packing in the complex **3** is significantly different from the others, due to the presence of bulky fluorine substituents, which are present in the flufenamic acid moiety. For each compound, the molecular packing along *b* vector is shown in Fig. 4.

The differences between crystal structures **1** and **2** versus **3** have also been observed in C—H···π stacking interactions between NSAIDs ligands and 1,10-phenanthroline ligands. Both **1** and **2** complexes show C—H···π hydrogen bonding interactions between the benzene rings of the tolfenamate (**1**) or mefenamate anions (**2**) as donor groups, and the pyridine-type rings of the 1,10-phenanthroline ligands, as acceptor groups. In contrast, the crystal structure of **3** shows a C—H···π hydrogen bonding interaction between the pyridine rings of the 1,10-phenanthroline ligands, functioning as donor groups, and the benzene rings of flufenamate anions, as acceptor groups (see Supplementary materials, Fig. S1).

3.2. Hirshfeld surface analysis

Hirshfeld surface analysis was used to study the intermolecular interactions within the crystal structure for all three complexes [36]. The 3D Hirshfeld surfaces for all complexes are illustrated in Fig. 5, which have been mapped over a d_{norm} shape index. The deep red spots on the d_{norm} Hirshfeld surfaces indicate the close contact interactions, which are mainly responsible for the significant intermolecular hydrogen bonding interactions and represent the C—H···O and C—H···π hydrogen bonding interactions [35]. For **1** and **3**, weaker C—H···Cl or C—H···F, respectively, hydrogen bonding interactions are evident.

The Hirshfeld 2D fingerprint plots of all complexes are illustrated in the Supplementary materials (see Figs. S2–S5) and allow a straightforward mapping of the significant intermolecular interactions on the molecular surface [47,48]. The 2D fingerprint plots indicate (Supplementary Figs. S2 and S4 for **1** and **2**), that the more dominant interactions are those of H···H type, which cover 42.2/38.7% (major/medium parts of disorder of **1**) of the total Hirschfeld surface.

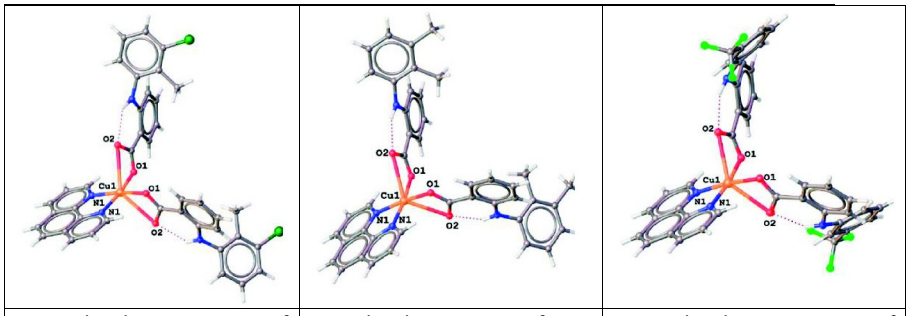

A: Molecular structure of complex [Cu(tolf-*O,O′*)$_2$(phen)] (**1**)

B: Molecular structure of complex [Cu(mef-*O,O′*)$_2$(phen)] (**2**)

C: Molecular structure of complex [Cu(fluf-*O,O′*)$_2$(phen)] (**3**)

Fig. 2. Molecular structures of complex **1** (A), complex **2** (B) and complex **3** (C).

Table 2
Selected bond lengths for [Cu(tolf-*O,O′*)$_2$(phen)] (**1**), [Cu(mef-*O,O′*)$_2$(phen)] (**2**) and [Cu(fluf-*O,O′*)$_2$(phen)] (**3**).

[Cu(tolf-*O,O′*)$_2$(phen)] (1)		[Cu(mef-*O,O′*)$_2$(phen)] (2)		[Cu(fluf-*O,O′*)$_2$(phen)] (3)	
Atom-atom	Bond length (Å)	Atom-atom	Bond length (Å)	Atom-atom	Bond length (Å)
Cu1-O1^1	1.919(3)	Cu1-O1	1.9331(12)	Cu1-O1	1.9470(14)
Cu1-O1	1.919(3)	Cu1-O1^1	1.9331(12)	Cu1-O1^1	1.9470(14)
Cu1-N1	2.009(4)	Cu1-N1	2.0153(15)	Cu1-N1	2.0040(17)
Cu1-N1^1	2.009(4)	Cu1-N1^1	2.0153(15)	Cu1-N1^1	2.0040(17)
Cu1-O2^{1,d}	2.734(12)	Cu1-O2	2.7054(13)	Cu1-O2	2.5708(14)
Cu1-O2A^d	2.942(13)	Cu1-O2^1	2.7054(13)	Cu1-O2^1	2.5708(14)
Cu1-O2B^d	2.60(2)				

Symmetry code: (1) i–x, *y*, 3/2–*z*; ^{d} Disordered carboxylate group.

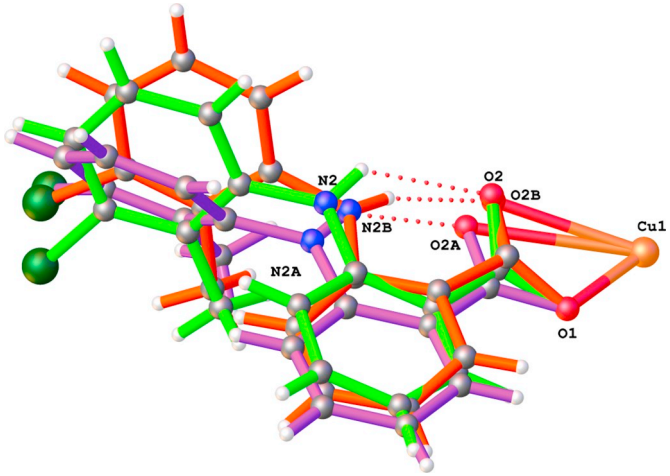

Fig. 3. A disordered tolfenamate anion in structure of complex [Cu(tolf-*O,O′*)$_2$(phen)] (**1**). Green, violet and orange bonds indicate three statical positions of tolfenamate anions. Atomic occupancy factors for all three positions are as follows: for Cu—O1 (2.735 Å) is 0.426(3), for Cu-O2A (2.940 Å) is 0.310(2) and for Cu-O2B (2.610 Å) is 0.264(3).

Contrastingly, the 2D fingerprint plots of H···H interactions in the crystal structure of **3** cover only 20.0% of the surface, and accordingly are less important. The 2D fingerprint plots of all three complexes (see Figs. S2–S5) show that the weak H···C/C···H hydrogen bonding interactions are in the range 24.6–34.9% of the total Hirshfeld surface and are the most significant interactions in the crystal. As shown in the Supplementary Figs. S2, S3 and S5, the scattered points in the 2D finger plots of **1** and **3** show additional H···Cl/Cl···H (**1**) or H···F/F···H (**3**) interactions, which cover 21.4% of the total Hirshfeld surface.

3.3. EPR spectroscopy

X-band EPR spectra of all three copper(II) complexes were studied both as polycrystalline solids and in fluid solutions at low temperature. Typically, the EPR spectra measured from frozen solutions were better resolved than those recorded from solid state samples [49]. An investigation was made to see whether the geometry around copper ion is influenced by the presence of a solvent.

3.3.1. Solid state EPR spectroscopy

Experimental EPR spectra (along with their computer simulations), recorded from complexes **1–3**, measured at 100 K in the solid state at X-band, are shown in Fig. 6. As is typical for magnetically concentrated systems, measurements at liquid nitrogen temperature did not show any improvements in the resolution of the EPR spectra. All EPR spectra in solid state can be interpreted using an effective $S = 1/2$ spin Hamiltonian [50]:

$$\hat{H} = g_{\|}\beta B_z \hat{S}_z + g_{\perp}\beta(B_x\hat{S}_x + B_y\hat{S}_y) + A_{\|}\hat{I}_z\hat{S}_z + A_{\perp}(\hat{I}_x\hat{S}_x + \hat{I}_y\hat{S}_y) \quad (4)$$

where the symbols have their usual meaning, and $S = 1/2$ and $I = 3/2$ for cupric d^9 ions.

The EPR spectrum of complex **1** (Fig. 6A), as measured in solid state, shows slightly rhombic symmetry and no observable hyperfine splitting. Considering the differences in bond lengths for the directly coordinated nitrogen atoms (from phenanthroline) and the oxygen atoms (from tolfenamic acid) to copper, and the departure of oxygen and nitrogen donors (2N2O) from a purely square planar arrangement, the observed weak rhombicity in the x-y plane is not surprising and accords with the X-ray structural characterization.

Even at high spectrometer gain, the half-field ("forbidden") transitions that are usually observed at around 1500 G were not observed [51], which is compatible with relatively high copper-copper distances (> 8 Å) and possible shielding effects of carboxylic acids. Both effects serve to reduce the magnetic dipole-dipole interactions between separate paramagnetic molecules, which assist the transition to occur.

The EPR spectrum of **2** (Fig. 6B) shows axial symmetry with a weakly resolved hyperfine interaction with copper nuclei, in the parallel direction, and similarly to complex **1**, we were also unable to detect a half-field transition, which accords with there being relatively large copper-copper distances (this is 8.286 Å for **2**) in the unit cell [52]. The mefenamic acid molecule contains two relatively bulky methyl groups, and so a ligand-shielding effect probably takes place, which

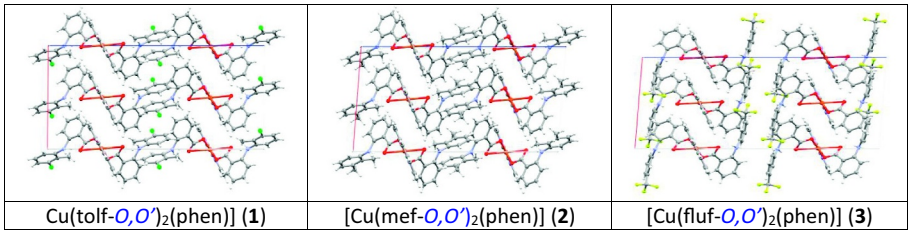

Fig. 4. Crystal packing for complexes **1–3** along *b* axis.

contributes to the suppression of the dipole-dipole interaction between the closest pair of copper atoms (8.286 Å) in the unit cell. This correlates with the observed weak in intensity parallel hyperfine splitting.

The EPR spectrum of complex **3** (Fig. 6C) is well resolved and shows a parallel hyperfine splitting pattern of 160 G, which is typical for a distorted ligand arrangement around a copper atom. The resolved hyperfine splitting indicates either a large copper-copper distance in the crystallographic cell (for **3** is 8.043Å) and/or more pronounced shielding effect of the carboxylate ligands. Regardless of the shortest copper-copper distance for complex **3**, (8.043Å; the differences in copper-copper distances are negligible), the observation of hyperfine splitting can be accounted for by the shielding effect due to the presence of the bulky fluorine atoms of flufenamic acid.

The EPR spectrum of complex **3**, measured at room temperature exhibits five hyperfine lines in the parallel direction (Fig. S6), which indicates the presence of two copper sites with slightly different coordination environments. Upon cooling to about 210 K, the pattern of five parallel hyperfine lines collapsed into the usual four line set, which indicates that a phase transition had occurred at this temperature. Below 210 K the EPR spectrum remained unchanged. The occurrence of the phase transition is apparent from the temperature dependence of the EPR spectra for **3**, which are shown in the Supplementary Material (Figs. S6 and S7).

Computer simulation revealed that all three complexes have $g_{\perp} < g_{||}$, which indicates that in all three complexes the unpaired electron is in the antibonding Ψ_{b1g} molecular orbital and so there is an elongated distorted tetragonal bipyramidal coordination around the copper atom, in agreement with the X-ray structural analysis.

The electronic spectra for all three complexes under study were measured in the solid state, using a Nujol suspension technique (spectra not shown). These exhibit intra-ligand (observed in the range of 360–300 nm) and ligand-to-metal charge-transfer (LMCT) absorptions (observed in the range of 310–360 nm) bands. In the spectral range 570–720 nm, forbidden *d-d* transitions were observed, as are typical for complexes with a distorted bipyramidal coordination around the copper (II) ion. The absorption wavelengths are as follows: complex **1** [592 nm (16,891 cm^{-1}), 717 nm sh (13,947 cm^{-1})]; complex **2** [577 nm (17,331 cm^{-1}), 720 nm sh (13,888 cm^{-1})]; complex **3** [601 nm (16,638 cm^{-1}), 711 nm sh (14,064 cm^{-1})].

When taken together with d-d transition frequencies, the EPR data can be used to estimate the MO coefficients, α^2 and β_1^2 and β^2, which characterize the degree of covalency in the σ-plane, π-in-plane, and π-out of plane bonding, respectively. Using an iterative solution of a set of equations [53] that connect the spin Hamiltonian parameters and *d-d* transitions, we were able to estimate values of the MO coefficients for complex **3** (which is the only complex with resolved parallel hyperfine splitting in its solid state EPR spectrum). The values obtained for complex **3** are $\alpha^2 = 0.83$, $\beta_1^2 = 0.73$ and $\beta^2 = 0.88$, which indicates an appreciable in-plane covalency in the *σ*- and π-bonding between the copper ion and the ligands in the equatorial plane. The value of β^2 indicates that the covalency of the out-of-plane π-bonding is slightly reduced.

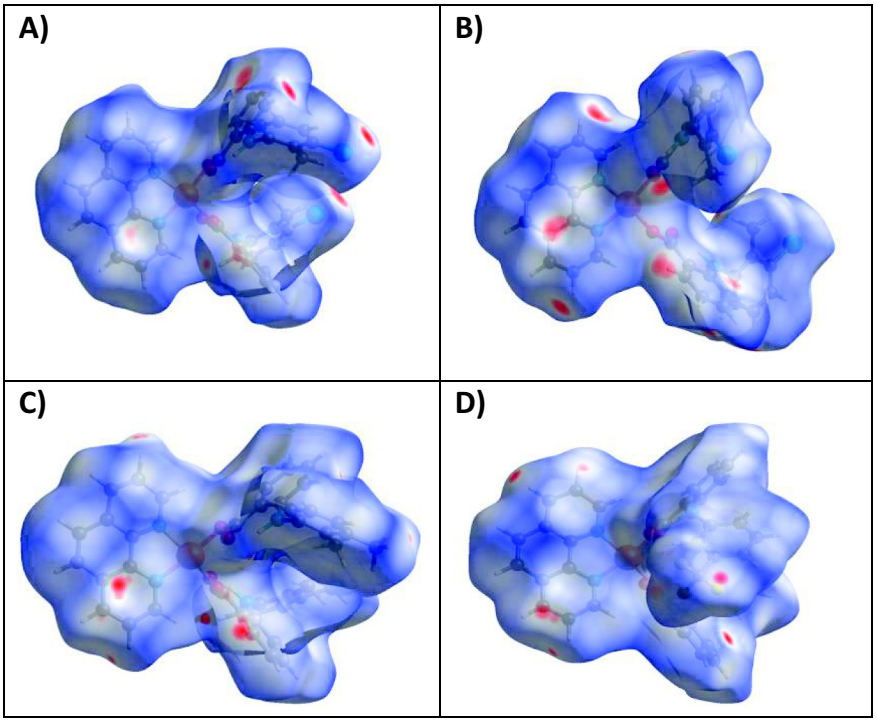

Fig. 5. A) View of the three-dimensional Hirshfeld surface of complex **1** (majority part of disorder) plotted over d_{norm} in the range −0.2815 to 1.2636 a.u. B) View of the three-dimensional Hirshfeld surface of complex **1** (medium part of disorder) plotted over d_{norm} in the range −0.2974 to 1.3695 a.u. C) View of the three-dimensional Hirshfeld surface of complex **2** plotted over d_{norm} in the range −0.1109 to 1.3467 a.u. D) View of the three-dimensional Hirshfeld surface of complex **3** plotted over d_{norm} in the range − 0.1123 to 1.3491 a.u. Legend: [Cu(tolf-*O*,*O*′)$_2$(phen)] (**1**), [Cu(mef-*O*,*O*′)$_2$(phen)] (**2**), [Cu(fluf-*O*,*O*′)$_2$(phen)] (**3**).

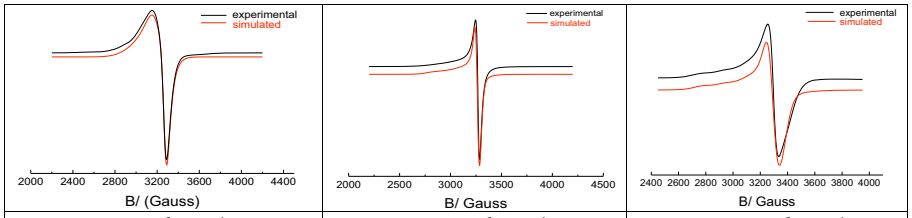

A: EPR spectrum of complex **1** measured in solid state. SH parameters: g_1 = 2.065, g_2 = 2.105, g_3 = 2.205, ΔB = (40, 135, 300) Gauss. Lorentz/Gauss = 0.1.

B: EPR spectrum of complex **2** measured in solid state. $g_{\perp}$ = 2.069, $g_{||}$ = 2.290, $A_{||}$ ~ 100 Gauss, ΔB = (35,35,120) Gauss, Lorentz/Gauss = 0.1.

C: EPR spectrum of complex **3** measured in solid state. SH parameters: g_1 = 2.070, g_2 = 2.070, g_3 = 2.261, A_1 = 10 Gauss, A_2 = 10 Gauss, A_3 = 160 Gauss, ΔB = (65, 70, 135) Gauss. Lorentz/Gauss = 0.05.

Fig. 6. X-band EPR spectra of complexes **1–3** and their computer simulations in solid state at 100 K. Legend: [Cu(tolf-*O,O′*)$_2$(phen)] (**1**), [Cu(mef-*O,O′*)$_2$(phen)] (**2**), [Cu(fluf-*O,O′*)$_2$(phen)] (**3**).

3.3.2. Solution EPR spectroscopy

The EPR spectra of metal complexes measured in frozen solutions are usually better resolved than those in the solid state, mainly due to the reduction of magnetic dipole-dipole and/or exchange interactions between adjacent molecules in the unit cell [54]. However, we must also be aware that the EPR data obtained from spectra measured in solutions may additionally reflect "solvent effects", especially when strongly coordinating solvents such as DMSO are present. In such cases we may expect a shift in the *g* and *A* values from those measured from the corresponding solid-state samples. Nonetheless, the better resolution of solution EPR spectra can provide more detailed information about the local environment around the metal center [55]. In addition, all biological experiments were carried out in the liquid phase, and so, the solution-phase EPR measurements are more compatible with actual biological media.

The EPR spectrum of complex **1** measured in frozen DMSO solution is shown in Fig. 7A, which displays a nicely resolved parallel hyperfine splitting pattern. It has been well established, particularly for CuX4 (and also for CuX2Y2) systems, that tetrahedral distortions of a planar CuX4 moiety markedly reduce $A_{||}$ while simultaneously increasing $g_{||}$. The tetrahedral distortion which is manifest by the dependence of $g_{||}$ on the dihedral angle led to the introduction of the quotient $g_{||}/A_{||}$ as a convenient measure of the degree of that distortion [56]. The EPR data, for the complex **1** provide a value of ~ 140 cm, which suggests a slight tetrahedral distortion around the copper atom, in agreement with the solid state X-ray data. Thus, if the conclusion derived from this parameter is consistent with the X-ray data obtained in solid state, we may conclude that the coordination geometry around the metal center is not significantly influenced by the presence of the solvent molecules (DMSO).

The EPR spectrum of complex **2** measured in DMSO solution at 77 K is shown in Fig. 7B, and similarly to complex **1**, it exhibits resolved hyperfine splitting. The EPR data suggest that complex **2** has a similar structure in the solid state as it does in DMSO solution. The calculation of the quotient $g_{||}/A_{||}$ for complex **2** gives 143 cm, which also suggests there is a weak distortion in its equatorial plane.

The EPR spectrum of complex **3** measured in frozen DMSO solution is shown in Fig. 7C. In agreement with the well-resolved EPR spectrum in the solid state, the solution EPR spectrum is nicely resolved. The appropriate calculation gives a value of about 140 cm, which is entirely consistent with the values obtained for complexes **1** and **2**. From the similarity of the EPR data obtained for complex **3** as a solid sample, and those determined from a frozen solution of the complex, it can be concluded that the same geometry is preserved and not affected by the solvent. This finding is important in drawing conclusions from biological experiments.

3.4. Electrochemical studies of the copper(II) complexes

Cyclic voltammetry measurements were made to explore the electrochemical behavior of the complexes **1**, **2** and **3**, across the entire potential range from −1.0 V to +1.5 V, using a scan rate of 100 mV/s [57]. Fig. 8 depicts the respective CV records for each compound measured separately at a concentration of 10^{-4} M, in the presence of 0.1 M NaCl, using a miniaturized boron-doped diamond (BDD) electrode. The resulting experimentally determined redox parameters of the complexes are summarized in Table 3. In Fig. 8, the distinct reduction waves can be seen in the cathodic scan with peak potentials ($E_{p,red}$) at −0.277 V, −0.305 V and −0.302 V for **1**, **2** and **3**, respectively, which reflect the redox conversion of Cu(II) to Cu(I), as held within the 1,10-

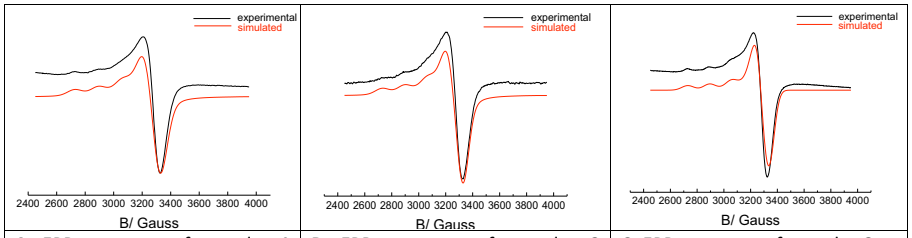

A: EPR spectrum of complex **1** measured in DMSO solution (1 mM) at 77 K. $g_{\perp}$ = 2.095, $g_{||}$ = 2.301, $A_{\perp}$ = 15 Gauss, $A_{||}$ = 166 Gauss, ΔB = (100, 100, 100) Gauss. Lorents/Gauss = 0.05.

B: EPR spectrum of complex **2** measured in DMSO solution (1 mM) at 77 K. $g_{\perp}$ = 2.098, $g_{||}$ = 2.301, $A_{\perp}$ = 15 Gauss, $A_{||}$ = 160 Gauss, ΔB = (80, 80, 90) Gauss. Lorents/Gauss = 0.2.

C: EPR spectrum of complex **3** measured in DMSO solution (1 mM) at 77 K $g_{\perp}$ = 2.090, $g_{||}$ = 2.295, $A_{\perp}$ = 15 Gauss, $A_{||}$ = 165 Gauss, ΔB = (60, 60, 90) Gauss. Lorents/Gauss = 0.2.

Fig. 7. Experimental EPR spectra of complexes **1–3** and their computer simulations measured in DMSO solutions (1 mM) at X-band at 77 K. 2nd order effects were applied in simulation. Legend: [Cu(tolf-*O,O′*)$_2$(phen)] (**1**), [Cu(mef-*O,O′*)$_2$(phen)] (**2**), [Cu(fluf-*O,O′*)$_2$(phen)] (**3**).

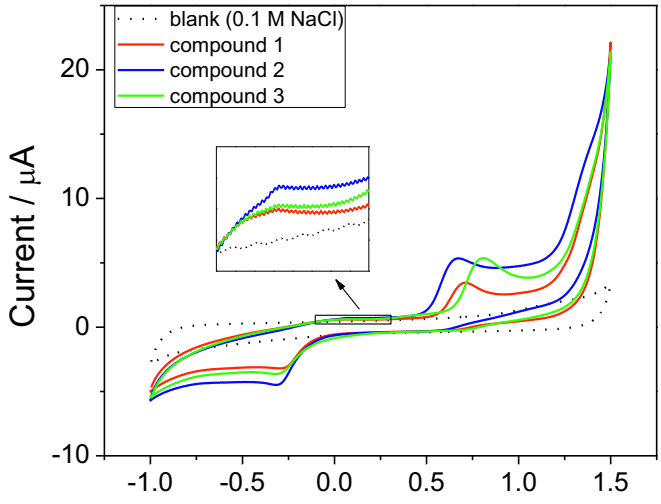

Fig. 8. CV records of studied complexes **1**, **2** and **3** (10^{-4} M) in 0.1 M NaCl at miniaturized BDD electrode using the scan rate of 100 mV/s. Legend: [Cu(tolf-*O*,*O*′)$_2$(phen)] (**1**), [Cu(mef-*O*,*O*′)$_2$(phen)] (**2**), [Cu(fluf-*O*,*O*′)$_2$(phen)] (**3**).

phenanthroline moiety of the copper-complexes. By application of an anodic scan, the corresponding, and weakly defined oxidation waves were recorded, with peak potentials ($E_{p,ox}$) at −0.036 V, −0.023 V and −0.036 V. These small peaks could be ascribed to the re-oxidation of Cu(I) to Cu(II), thus indicating the quasi-reversible nature of the electrode reactions of all the substances studied using the BDD electrode. The redox behavior (shapes of the CV traces) of the compounds studied all appeared to be similar, which thus confirmed their structural congruence. However, differences in the overall electrochemical activity of the complexes was attested to, by the presence of striking oxidation signals with current responses at +0.704 V (1.935 μA), +0.653 V (3.018 μA) and +0.794 V (3.019 μA) for **1**, **2** and **3**, respectively. The latter might be related to the redox activity of the bis(tolfenamato)-, bis(mefenamato)- and bis(flufenamato)- moieties in **1**, **2** and **3**, respectively. As evidenced from the values of the redox parameters shown in Table 3, it can be concluded that the peak potential of +0.794 V (green curve in Fig. 8) measured for **3** was the highest among all the substances studied. This phenomenon might be explained by the presence of the "bulky" bis(flufenamato)- moiety within the structure, with a strong electron-withdrawing ability which impedes mass transport during the redox reaction of this moiety at the miniaturized BDD electrode.

As can be seen from the Table 3, the differences in Cu(II)/Cu(I) redox potentials between complexes **1**, **2** and **3** are negligible which accords with the similarity in coordination environments around the copper(II) ions as revealed by X-ray diffraction measurements. The effect of the distant substituents (chlorine in **1**, methyl in **2** and fluorine in **3**) on the redox properties of the copper(II) complexes has been found to be small. The values of $E_{1/2}$ for all three complexes are within the range (−0.363 and 0.687 V vs Ag/AgCl), which is required for an effective dismutation of the superoxide radical anion by copper(II) complexes to occur. The results of SOD mimetic activity for all three complexes are presented in Section 3.6.

In addition, the CV record of the supporting electrolyte (0.1 M NaCl) confirmed that the background current was observed at very low levels with the miniaturized BDD electrode over the whole potential range. This demonstrates that this particular working electrode material is a good choice with which to study the electrochemical behavior of miscellaneous structurally and biologically relevant complexes [57].

3.5. DNA interaction studies

The binding of metal complexes with the DNA (along with a myriad of other targets that exist in living cells) is regarded to be one of the possible mechanisms responsible for their cytotoxic potential. In principle, there exist two modes for binding the metal complexes to DNA: covalent [58] and non-covalent - (which includes electrostatic interactions, groove binding and intercalation between base pairs) [59]. An elucidation of the relationship of the DNA - metal complex binding mode vs biological activity provides significant information to aid the design of new metal complexes, targeted to DNA, with an improved therapeutic potential. In the present work, the interaction of the synthesized complexes **1–3** with calf-thymus DNA was studied using both absorption titrations and viscometry.

3.5.1. Absorption titrations

Electron absorption titrations provide the most commonly used method to detect the mode and strength of the interaction of metal complexes with the DNA molecule. Any change in the spectrum of the complex (absorbance, wavelength shift) following the addition of the DNA is considered to provide evidence of an interaction occurring between the added substance and DNA. Hyperchromic and hypochromic shifts in the spectrum reflect changes in the secondary DNA structure. Hyperchromism indicates any destabilization of the DNA structure, while hypochromism is associated with the stabilization of DNA secondary structure by the electrostatic interactions or intercalation of metal complex [59–61]. The hypochromic and bathochromic shifts in the spectrum are associated with an intercalation mechanism that involves the insertion of a planar molecule between the DNA base pair and the subsequent DNA prolongation and stabilization [62–65]. It has been reported that in a typical case of intercalation of metal complex into a strand of DNA, hypochromic and bathochromic shifts were > 35% and > 15 nm, respectively [63,66]. Since the intercalation mechanism involves a stacking interaction between aromatic chromophores and DNA base pairs, the extent of hypochromism is usually consistent with the degree of intercalation interaction [67].

The absorption spectra of the complexes **1–3** in the absence and presence of CT-DNA in 5 mM Tris-HCl and 50 mM NaCl at pH 7.2 are shown in Fig. 9. The spectra were recorded at a constant concentration of a complex compound using different ratios of Cu-complex to CT-DNA concentrations ([Cu-complex]/[DNA]). The absorption spectra of all complexes are very similar and exhibit three maxima with the best resolved band being observed at 274 nm (Table 4). As the concentration

Table 3
Redox parameters of studied complexes **1–3** evaluated by cyclic voltammetry. Legend: [Cu(tolf-*O*,*O*′)$_2$(phen)] (**1**), [Cu(mef-*O*,*O*′)$_2$(phen)] (**2**), [Cu(fluf-*O*,*O*′)$_2$(phen)] (**3**).

Redox parameters	Cu(II)/Cu(I)						Ligand	
Studied compound	$E_{p,ox}$	$E_{p,red}$	$E_{1/2}$	ΔE	$I_{p,ox}$	$I_{p,red}$	$E_{p,ox}$	$I_{p,ox}$
	V				μA		V	μA
1	−0.036	−0.277	−0.157	0.241	0.321	−1.611	+0.704	1.935
2	−0.023	−0.305	−0.164	0.282	0.447	−2.423	+0.653	3.018
3	−0.036	−0.302	−0.169	0.266	0.341	−1.561	+0.794	3.019

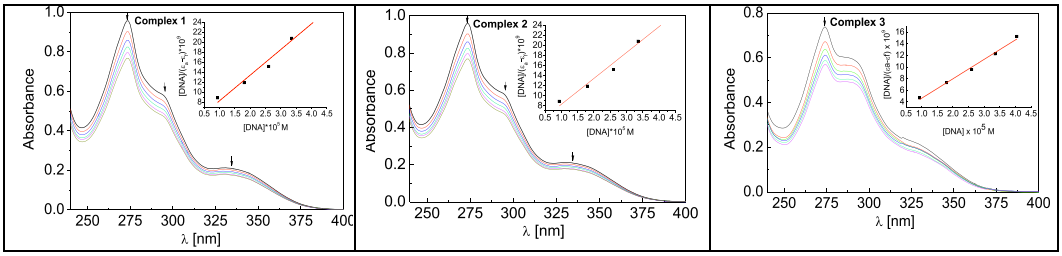

Fig. 9. UV–Vis absorption spectra of complexes (1–3) in the absence and presence of CT-DNA in 5 mM Tris-HCl, 50 mM NaCl at pH 7.2. Concentration of complexes was kept constant (20 μM) and concentration of DNA varied from 0 to 60 μM. Legend: [Cu(tolf-*O*,*O*′)$_2$(phen)] (**1**); [Cu(mef-*O*,*O*′)$_2$(phen)] (**2**); [Cu(fluf-*O*,*O*′)$_2$(phen)] (**3**).

of CT-DNA increases, the intensity of the absorption bands was found to decrease to different degrees (Table 4). In the UV spectrum of **1** (Fig. 9), the bands centered at 274, 295, and 330 nm exhibit a hypochromism of ~ 25.3, 20.5, and 17.3%, respectively. In the UV spectrum of **2**, the bands centered at 273, 295, and 330 nm exhibit a hypochromism of ~ 19.9, 17.9, and 15.1%, respectively. Finally, in the UV spectrum of **3**, the bands centered at 274, 290, and 330 nm exhibit a hypochromism of ~ 22.7, 17.9, and 20.2%, respectively.

Though the exact mode of complex – DNA interaction cannot be proposed based on these UV spectroscopic studies alone, the changes in absorption spectrum of each complex clearly indicates that binding to DNA has occurred. The hypochromic shift can arise due to π-π* stacking interactions between aromatic chromophores of respective complex and DNA base pairs [68] and could be considered as providing initial evidence that a complex – DNA interaction has occurred, probably via the intercalative binding mode [59].

A quantitative determination of the binding strength of the complex to DNA, is made by measuring the internal binding constant (K_b) of the complex [69]. Therefore, binding constants (K_b) were determined for the complexes **1–3** with CT-DNA, as calculated according to Wolfe–Shimmer equation (Eq. (1)). These are given in Table 4. The K_b values are all of the order of $10^5\ M^{-1}$ and are considered to be an indicator of a relatively strong interaction occurring between DNA and the Cu(II) complexes [61]. The complexes can be ranked in the following order: **3** > **2**~**1**, in terms of the strength of their interaction with DNA.

3.5.2. Viscometric study

The binding mode for the Cu(II) complexes with DNA was further evaluated by means of viscosity measurements [70]. Changes in DNA viscosity are related to changes in the DNA strand length, which result from its interaction with a transition metal complex. A classical intercalation binding mode causes a separation of the DNA base pairs and a consequent elongation of the DNA molecule with an increase in its viscosity [61,71,72]. In contrast, the binding of a compound by means of a partial and/or non-classical intercalation mechanism can cause a bend or kink in the DNA helix, which decreases the effective strand length and results in a concomitant decrease (or absence of a change) in the viscosity of the DNA solution [73–75].

The effect of complexes (**1–3**) on the viscosity of CT-DNA is illustrated in Fig. 10. Ethidium bromide (EB, 3,8-diamino-5-ethyl-6-phenylphenantridium bromide), which is a planar, cationic molecule and well known for its excellent ability to intercalate into the DNA strand

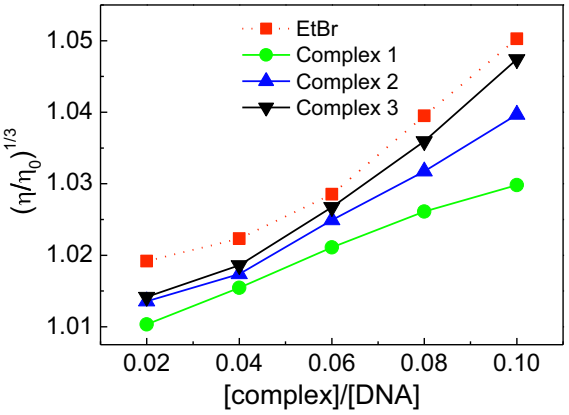

Fig. 10. Relative viscosity of CT-DNA in buffer solution (5 mM TRIS, 50 mM NaCl, pH 7.2) influenced by increasing amount of complexes (**1–3**) at 25 ± 0,1 °C compared to EtBr. Legend: [Cu(tolf-*O*,*O*′)$_2$(phen)] (**1**); [Cu(mef-*O*,*O*′)$_2$(phen)] (**2**); [Cu(fluf-*O*,*O*′)$_2$(phen)] (**3**).

and undergo π-π interactions with the nitrogen DNA bases [76], was used as a reference molecule. As can be seen from Fig. 10, the addition of the complexes (**1–3**) to a solution containing DNA results in a significant increase in its relative viscosity, which indicates that the relative intercalating ability of the complexes is in the order **3** > **2** > **1** and is in agreement with the absorption titrations (see above). It is reasonable to assume that the process is mediated via the very effective intercalating ligand, 1,10-phenanthroline, which projects away from the copper center, and can π-stack within the DNA helix. The phenanthroline moiety thus acts as an anchor for the whole complex and brings two bulky NSAID carboxylic acid molecules, both bound to the copper atom from opposite sides, into closer proximity with the DNA. The intercalation efficiency, and consequent unwinding of the helix will depend on the arrangement of the aromatic rings of the NSAID carboxylic acids and the orientation of substituents attached to them, which can interact with the DNA strand. In terms of the molecular structures of the complexes, it can be seen that in complex **3**, (in contrast to **1** and **2**), the plane of the substituted aromatic ring is slightly inclined, and the fluorine atoms are oriented toward the direction of intercalation to the DNA. We therefore propose, that this orientation might allow the formation of weak hydrogen bonds between the

Table 4
Decrease in the absorption spectra intensities for complexes **1–3** following interaction with CT-DNA expressed in % and calculated intrinsic binding constants (K_b) according to Wolfe–Shimmer equation. Legend: [Cu(tolf-*O*,*O*′)$_2$(phen)] (**1**); [Cu(mef-*O*,*O*′)$_2$(phen)] (**2**); [Cu(fluf-*O*,*O*′)$_2$(phen)] (**3**).

Complex	Band 1/nm	Decrease in absorption intensities/ %	Band 2/nm	Decrease in absorption intensities/ %	Band 3/nm	Decrease in absorption intensities/ %	K_b
1	274	25.3	295	20.5	~ 330	17.3	9.1×10^4
2	273	19.9	295	17.9	~ 330	15.1	1.6×10^5
3	274	22.7	290	17.9	~ 330	20.2	2.6×10^5

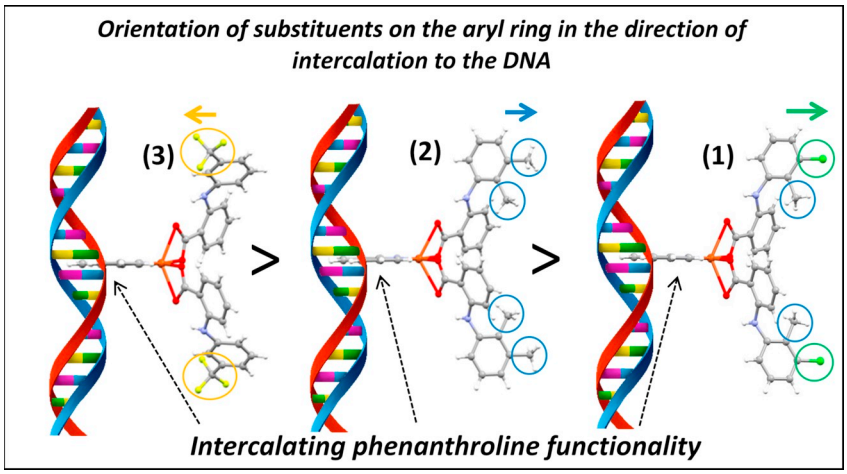

Fig. 11. Proposed orientation of aryl substituents of the complexes **1–3** in their interaction with DNA. (Only fluorine atoms (complex **3**) are oriented in the direction of intercalation to the DNA). Fluorine atom may act as a hydrogen bond acceptor. Legend: [Cu(tolf-*O*,*O*′)$_2$(phen)] (**1**); [Cu(mef-*O*,*O*′)$_2$(phen)] (**2**); [Cu(fluf-*O*,*O*′)$_2$(phen)] (**3**).

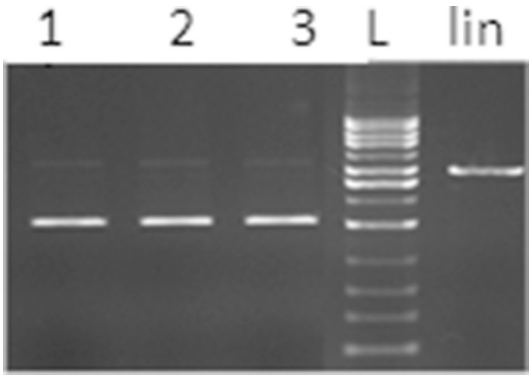

Fig. 12. Agarose gel (0.8%) showing the effect of H_2O_2 and DMSO on the conformation of plasmid DNA pBSK+ in a volume of 15 μl with 1 h incubation at 37 °C. Lane 1: SC form of pDNA (control), lane 2: pDNA in the presence of hydrogen peroxide, lane 3: pDNA in the presence of DMSO, L: 1 kb standard linkage: linear pDNA digested with restriction endonuclease EcoR1.

electron pairs of three fluorine atoms and hydrogen atoms at the surface of DNA. An ability of the fluorine atoms to form weak hydrogen-like interactions will favour those conformational changes that result in the stabilization of the interaction between complex **3** and DNA (see Fig. 11). The strength of hydrogen bonds, involving functional groups containing fluorine atoms was previously determined using a combination of NMR spectroscopy and theoretical calculations [77]. It has been proposed that intermolecular interactions in which fluorine acts as a hydrogen bond acceptor may have a significant biological relevance, particularly for the design of new drugs. Fluorine may act as a hydrogen bond acceptor or as a hydrophobic moiety (amphiphatic property) which results in different types of interactions in biological systems.

3.5.3. Nuclease activity of copper(II) complexes and mechanism of DNA damage

Chemical nucleases are metal complexes, that are capable of causing DNA cleavage by oxidative attack on the deoxyribose moiety, of which the first demonstrated example was copper(II)-1,10-phenanthroline [78]. Mono- and bis-(1,10-phenanthroline) Cu(II) complexes do not generate ROS. The DNA damage is achieved by an oxidation mechanism mediated by copper – oxo and hydroxo species that are capable of hydrogen abstraction at the C1′ position, which is augmented by oxidation at the C4′ and C5′ positions in DNA [79–82]. The nuclease activity of metal (copper) complexes is generally influenced by the intercalating behaviour of metal-complexes [78,82].

All three complexes **1–3** contain coordinated both 1,10-phenanthroline functionality to promote intercalation and NSAIDs tolfenamic, mefenamic and flufenamic acids as redox cycling functionalities. As already noted, copper(II) complexes containing NSAIDs are efficient scavengers of superoxide radical anions (SOD mimetics) and undergo redox-cycling between Cu^{2+} and Cu^{+} oxidation states ($Cu^{2+} + O_2\cdot^- \rightarrow Cu^{+} + O_2$), during which process, additional ROS such as hydroxyl radicals are formed which may further act as agents to promote DNA cleavage.

A very efficient technique with which to monitor the nuclease activity of metal complexes is gel electrophoresis. The reaction mixture contains the complex under study in the presence of plasmid DNA (pDNA), which is a covalently closed circular (CCC) DNA, that can occur in several different conformational states, predominantly the super-spiralized form known as SC (Supercoiled). When it is in the SC form a pDNA molecule moves most quickly in the electric field, but any change in conformation, or disruption in covalent bonding in one or both DNA strands, results in new forms of DNA with different mobilities through the gel [83]. If the covalent bond in one strand is broken, an "open" circular form is formed (OC, Open Circular) which is alternatively referred to as a "nicked" form. When covalent bonds are broken in both DNA strands, a linear form results.

The complexes **1–3** were dissolved in DMSO in a concentration ranging from 5 to 50 μM and studied either alone, or in the presence of hydrogen peroxide; it was found that neither hydrogen peroxide nor DMSO caused any changes in the conformation of pDNA (Fig. 12, lanes 2, 3).

The observed bands of the OC form of DNA (cleavage of a covalent bond in one pDNA fiber) in their electrophoretic profiles, indicate the ability of the complexes **1–3** to cleave pDNA even in the absence of hydrogen peroxide (Fig. 13, lanes 1–5).

That the DNA cleaving effect is strongest for the complex **3** is documented by the presence of intense bands from the corresponding OC form of pDNA. For the other two complexes, the intensity of the bands decreases in the order **2** > **1** (Fig. 13, lanes 1–5). This observed order of activity for the copper(II) complexes toward DNA cleavage (**3** > **2** > **1**), is in agreement both with the viscosity measurements (see Fig. 10) and absorption titrations (Table 4), which confirmed the highest value of intrinsic binding constant for complex **3** ($K_b = 2.6 \times 10^5$) which contains fluorine atoms.

Based on these results we can assume that the studied complexes act as intercalators due to the presence of the aromatic planar phenanthroline functionality. The DNA cleaving ability of the complexes **1–3** to cause a single strand DNA break correlates with their intercalating efficiency [84]. The relative binding strength of the complexes toward DNA is an important factor in their mechanism of action. We propose that the interaction of Cu(II) complexes **1–3** with the SC form of DNA in the absence of a reducing agent (hydrogen peroxide) leads to a mechanical unwinding of the helix.

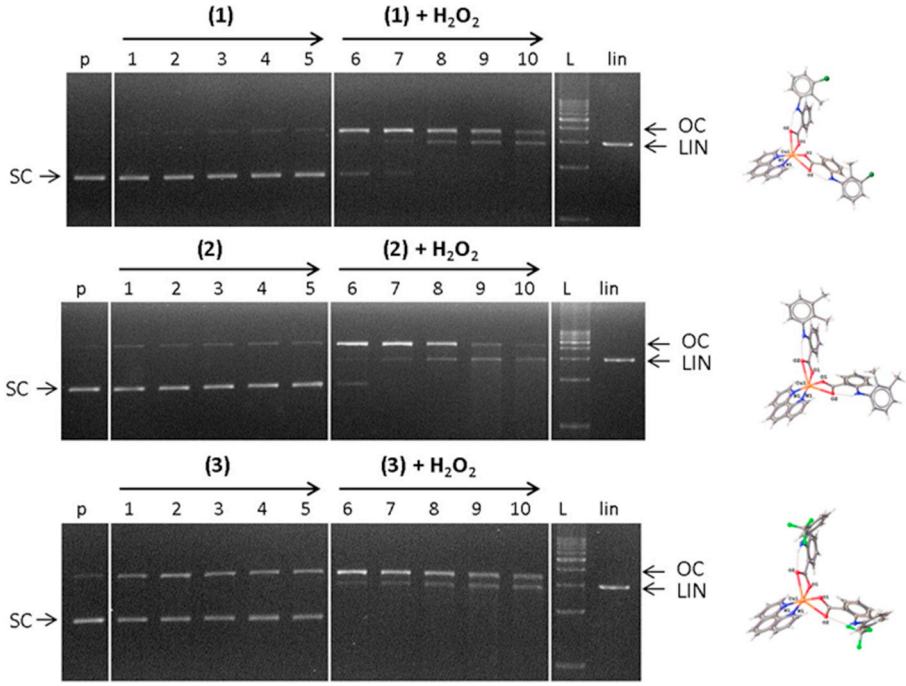

Fig. 13. Agarose gel (0.8%) showing the ability of complexes **1–3** to cleave plasmid DNA pBSK+ in the absence of H_2O_2 (lanes 1–5) and in the presence of H_2O_2 (lanes 6–10) in a 15 µl reaction mixture, incubated for 1 h at 37 °C. Lane p: SC form of pDNA (control), lanes 1–5: complexes **1–3** (concentrations 5; 10; 25; 40; 50 µM) incubated with pDNA, lanes 6–10: complexes **1–3** (concentrations 5; 10; 25; 40; 50 µM) incubated with pDNA and H_2O_2 (double concentration with respect to complexes **1–3**); L: standard 1 kb linear DNA; lin: linear pDNA after cleavage with the EcoR1 restriction endonuclease. Legend: [Cu(tolf-*O*,*O*′)$_2$(phen)] (**1**); [Cu(mef-*O*,*O*′)$_2$(phen)] (**2**); [Cu(fluf-*O*,*O*′)$_2$(phen)] (**3**).

Under simulated Fenton reaction conditions [85], i.e. in the presence of hydrogen peroxide, pDNA cleavage was observed with all three complexes **1–3** (Fig. 13, lanes 6–10). This is documented by the concentration-dependent effect of conversion of the SC form of DNA, first to the OC form and then further, to the linear form. Based on the intensity of the bands belonging to the individual pDNA conformations, we can also infer that the activities of the studied complexes are in the order **3** > **2** > **1**.

A clear concentration dependence was established, since at the two lowest concentrations of complex **1** (5 and 10 µM), some proportion of SC pDNA was preserved (Fig. 13, lanes 6, 7) and only at higher concentrations the complete conversion of SC DNA occurred (Fig. 13, lanes 8–10). Complex **2** exhibits a slightly higher activity but only preserves some of the SC form of DNA at the very lowest test concentration (lane 6). Complex **3** causes complete relaxation of the OC form even at the lowest (5 µM) concentration, which is observed in the gel as a complete loss of the SC band of pDNA (Fig. 13, lane 6).

The cleavage of pDNA in the reaction mixture containing the complexes **1–3** and hydrogen peroxide (simulated Fenton reaction), suggests that an oxidative (radical) DNA damage mechanism operates. The ability of copper complexes to produce ROS in the presence of hydrogen peroxide is considered to be one of the important mechanisms of their antitumor activity. ROS-induced DNA damage results predominantly from the redox-cycling (Cu(II)/Cu(I)) and catalytic activity of copper ions [84].

$$L - Cu(II) + H_2O_2 \rightarrow L - Cu(I) + O_2^{\bullet -} + 2H^+ \quad (5)$$

$$L - Cu(I) + H_2O_2 \rightarrow L - Cu(II) + OH^{\bullet} + OH^- \quad (6)$$

Assuming a weak non-covalent interaction between the phenanthroline moiety of the complexes **1–3** and DNA, we may propose that the redox reactions associated with ROS formation occur close to the DNA, which encourages strand breaking via the cleavage of covalent bonds (Fig. 14).

To identify the kind of ROS formed, various specific ROS scavengers (L-Histidine for singlet oxygen, DMSO for the hydroxyl radical and SOD for the superoxide anion radical) were added to the reaction mixture containing hydrogen peroxide and the highest concentration of the complex (50 µM) for which the greatest nuclease activity was found (Fig. 15). The representative electrophoretic profile in Fig. 15 shows results for complex **2** with different ROS traps added. As expected, the system containing the components of the Fenton reaction, cupric chloride and hydrogen peroxide (reference profile), caused complete conversion of the SC form of the pDNA to the OC form and the linear form (Fig. 15, lane 1). The effect of the added scavengers (Fig. 15, lanes 2–4) was compared against the reference profile (line 1).

Significant inhibition of pDNA cleavage was observed after addition of the SOD enzyme (Fig. 15, lane 4), which documents the significant production of the superoxide radical anion. A reduction in the intensity of the band corresponding to the preserved SC form of the pDNA, following the addition of L-histidine, demonstrates the formation of singlet oxygen in the reaction mixture (lane 2). Then by the addition of DMSO, an appreciable formation of hydroxyl radicals was confirmed in the gel, since only a minor loss of the linear form of pDNA (lane 3) was observed. These results confirm that the radical/oxidation mechanism of DNA damage occurs in the presence of the complexes **1–3**.

3.6. SOD-mimetic activity of copper(II) complexes

The SOD mimetic activity of the complexes (**1–3**) was determined using an indirect xanthine oxidase (XO) enzyme method in the presence of its natural xanthine substrate (X) [43]. The X/XO enzyme system serves as the source of the superoxide radical anion ($O_2^{\bullet -}$), which is scavenged by tetrazolium blue (Nitro-Blue-Tetrazolium (NBT)) and subsequently reduced to a blue-colored formazan. During the course of the reaction, the yellow color of the solution gradually changes to blue, as a result of NBT reduction. The change in color intensity correlates with the concentration of reduced NBT, i.e. with the amount of superoxide radical anion that has been scavenged. This color change is accompanied by the increase in the intensity of the absorption band at 550–560 nm [43].

When a substance, capable of scavenging superoxide radical is added to the reaction mixture, a competitive reaction takes place, which results in the inhibition of the reaction between NBT and the superoxide radical anion. The slowing of the NBT reduction or its complete termination results in a decrease in its spectral absorbance, which is proportional to the increasing concentration of the added substance (inhibitor). Thus, the rate of the change of absorbance intensity after the addition of the studied complexes was measured, and

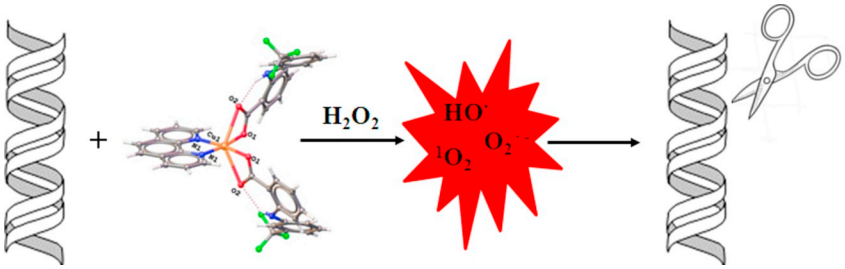

Fig. 14. Predicted mechanism of oxidative DNA damage.

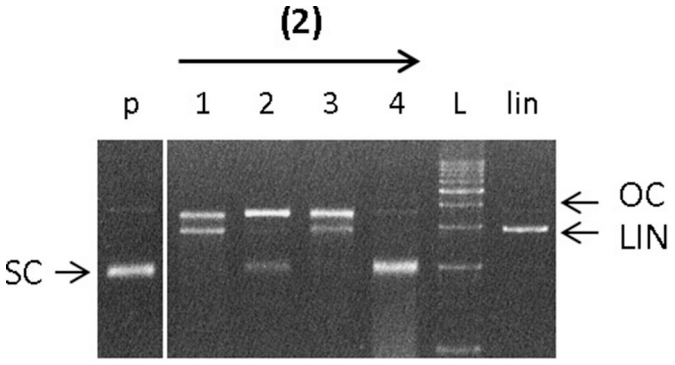

Fig. 15. Agarose gel electrophoresis (0.8%) of plasmid DNA pBSK+ with complex [Cu(mef-*O*,*O*′)$_2$(phen)] (**2**) (50 μM concentration) in the presence of H_2O_2 (concentration 100 μM) and after addition of radical scavengers (L-histidine (20 mM), DMSO (6 μl), SOD (15 U)). The reaction mixture is in a final volume of 15 μl, incubated for 1 h at 37 °C. Lane p: SC form of pDNA (control); lane 1: pDNA + complex **2** + H_2O_2; lane 2: pDNA + complex **2** + H_2O_2 + L-his; lane 3: pDNA + complex **2** + H_2O_2 + DMSO; lane 4: pDNA + complex **2** + H_2O_2 + SOD.

the IC_{50} values (concentration of the complex causing 50% inhibition of the NBT reduction) were determined from the graphical dependence of the rate of NBT reduction (% inhibition) on the concentrations of the complexes (Fig. 16). The results are shown in Table 5.

It is clear that all three complexes exhibit excellent SOD-mimetic activity, with IC_{50} values ranging from 0.94 to 1.23 μM (the smaller the value, greater the SOD-mimetic activity). The SOD-mimetic activity of complexes **1–3** decreases in order **3**∼**1** > **2**. To assess the effectiveness of SOD mimetic activity, we compared our results with the IC_{50} values of some anti-inflammatory drug complexes which were determined using the NBT assay under the same conditions (Table 5). The IC_{50} values obtained for the complexes **1–3** indicate that their SOD mimetic activities are within the same range as for other compounds which are known to possess excellent superoxide radical-scavenging activities. For comparison, the SOD activity of Cu(II)-indoctain complex, [$Cu_2(indo)_4(H_2O)_2$] is considered an excellent SOD mimetic,with an IC_{50} value of 1.31 μM [86]. Indomethacin (indoH) is an acid [1-(4-chlorobenzoyl)-5-methoxy-2-methyl-1H-indole-3-acetic acid] used orally as a highly effective anti-inflammatory drug in veterinary medicine. The studied complexes **1–3** show a greater SOD activity than was determined for the Cu(II)- indomethacin complex. A lower SOD-mimetic activity than that observed for complexes **1–3** was reported for

Table 5
Superoxid dismutase (SOD) mimetic activity of complexes **1–3** and selected examples.

Complex	IC_{50} [μmol·dm^{-3}]	References
[Cu(tol-*O*,*O*′)$_2$(phen)] (1)	**0.98**	**This work**
[Cu(mef-*O*,*O*′)$_2$(phen)] (2)	**1.23**	**This work**
[Cu(flu-*O*,*O*′)$_2$(phen)] (3)	**0.94**	**This work**
[Cu(tolf)$_2$H$_2$O]$_2$	1.97	[43]
[Cu(tolf)$_2$DMF]$_2$	2.13	[43]
[Cu(Nap)$_4$(3-pym)$_2$]*n*	0.39	[87]
[Cu(sal)(phen)]	1.01	[84]
[Cu_2(Indo)$_4$(phen)](H$_2$O)$_2$	1.31	[86]
Native SOD	0.04	[88]

Cu(II)-tolfenamic acid complexes [Cu(tolf)$_2$H$_2$O]$_2$ and [Cu(tolf)$_2$DMF]$_2$ [43]. This indicates that, in addition to importance of NSAID tolfenamic acid, an auxiliary ligand (in our case intercalator phenanthroline) may also play a significant role in the SOD-mimetic activity of the metal complexes.

The mechanisms of the SOD mimetic activity of low-molecular weight Cu(II) complexes can be proposed as follows. First, the superoxide radical anion ($O_2\cdot^-$) binds to the Cu(II) ion of the complex, followed by electron transfer from the superoxide radical anion to Cu (II) (Eq. (7)). The resulting cuprous complex, Cu(I)-L, undergoes redox cycling and is oxidized back to the cupric complex, Cu(II)-L, by a reaction with another molecule of $O_2\cdot^-$ (Eq. (8)) [87]:

$$Cu(II) - L + O_2^{\cdot -} - \rightarrow Cu(I) - L + O_2 \quad (7)$$

$$Cu(I) - L + O_2^{\cdot -} + 2H^+ \rightarrow Cu(II) - L + H_2O_2 \quad (8)$$

The SOD mimetic activity of Cu(II) complexes is affected by a number of factors of which the most critical are: (i) minimal steric barriers to the superoxide radical anion accessing the copper ion and (ii) the rapid exchange of axially coordinated ligands to the copper(II) ion. Considering the fact that the complexes **1–3** exhibit minimal structural differences, it is reasonable to assume that the small differences in SOD mimetic activity may originate in the nature of the distant substituents on the aryl ring (chlorines in complex **1**, methyl groups in complex **2** and fluorines in complex **3**) and slight differences in the geometry of copper(II) cores of all three metal complexes.

To obtain direct experimental evidence for the reduction of Cu(II) complexes by superoxide radical anions, a specific chelator of Cu(I) species, neocuproine was introduced. Cu(I) forms a colored complex with neocuproine (Cu(I)-neocuproine) that absorbs at 458 nm [89]. The

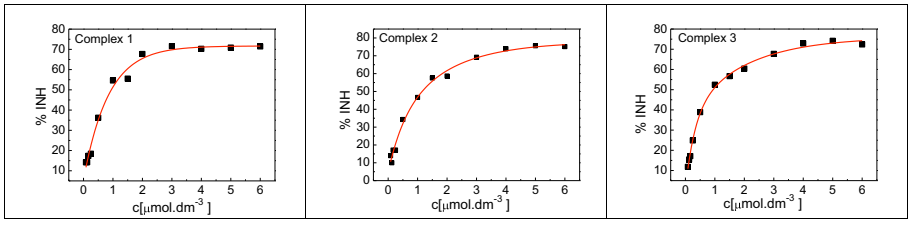

Fig. 16. Dependences of the NBT reduction by superoxide radical anion (% Inhibition) on the concentration of complexes **1–3**. Legend: [Cu(tolf-*O*,*O*′)$_2$(phen)] (**1**); [Cu(mef-*O*,*O*′)$_2$(phen)] (**2**); [Cu(fluf-*O*,*O*′)$_2$(phen)] (**3**).

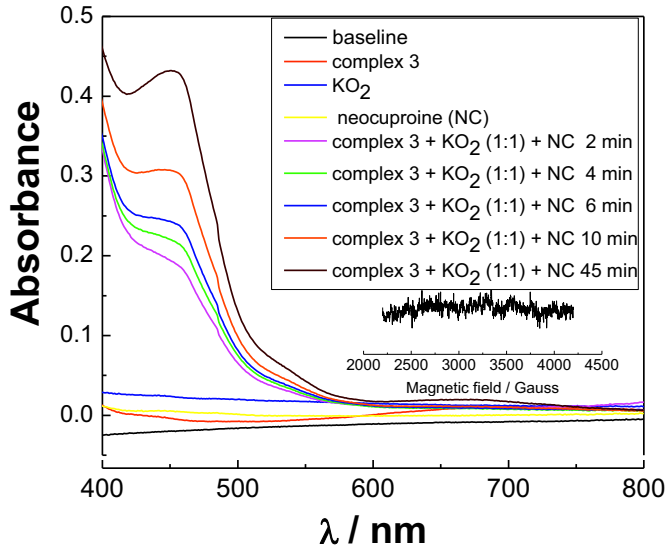

Fig. 17. Absorption spectra of the interaction of complex **3** and KO_2 (1:1) in DMSO in the presence of neocuproine (NC) showing time dependent increase of the absorbance of Cu(I)-neocuproine complex. Inset: The EPR silent spectrum of the corresponding system measured after 2.5 h showing complete reduction of paramagnetic Cu(II) to diamagnetic – EPR silent Cu(I).

time dependent increase of the absorption band at 458 nm observed following mixing of the Cu(II) complexes **1–3** with superoxide radical anions (KO_2) in the presence of neocuproine confirms that reduction of Cu(II) to Cu(I) and formation of Cu(I)-neocuproine complex has occurred (Fig. 17). Cu(I) contains 10 paired *d* electrons and is therefore EPR silent (no signal); hence, the absence of an EPR signal from complex **3**, as recorded after 2.5 h, confirmed that the complete reduction of Cu(II) to Cu(I) had occurred (see inset, Fig. 17). The redox cycling mechanism was thus confirmed for Cu(II) in all complexes **1**, **2** and **3** in the presence of superoxide radical anion (Eqs. (7) and (8)), and this cycling between cupric and cuprous species (Cu(II) → Cu(I) → Cu(II)) explains the formation of superoxide radical anions, hydroxyl radicals and singlet oxygen, all of which contribute to DNA damage (see above).

3.7. Interaction of copper(II) complexes with albumin

Human serum albumin (HSA) is the most abundant protein in blood plasma present in millimolar concentrations. HSA is involved in the transport of metal ions, metal-complexes, drugs and fatty acids, and contains tryptophan at the amino acid position 214, which exhibits an intense fluorescence emission at 347 nm upon excitation at 295 nm. The quenching of the HSA fluorescence in the presence of complexes **1–3** is shown in Fig. 18. Fluorescence quenching is a consequence of binding of the complexes **1–3** to tryptophan residues in HSA which causes conformational changes of albumin, subunit associations, denaturation or substrate binding [90]. The observed quenching (up to 98% for complex **3**) of the initial fluorescence intensity clearly demonstrates that binding of copper(II) complexes to the albumin has occurred. The values of K_{sv} and k_q for the interaction of complexes **1–3** with albumin have been obtained by means of the Stern–Volmer equation (Eq. (2)). The values of the association binding constants (*K*) and the number of binding sites per albumin (*n*) have been calculated using the Scatchard equation (Eq. (3)). The data thus obtained are summarized in Table 6 and indicate that complex **3** has the strongest quenching ability ($k_q = 2.24 \times 10^{14}\ M^{-1}\,s^{-1}$). The values obtained are several orders of magnitude greater than those for typical biopolymer fluorescence quenchers ($k_q \sim 10^{10}\ M^{-1}\,s^{-1}$) which indicates that the mechanism of static quenching operates [20,90].

The relatively high values obtained for the association binding

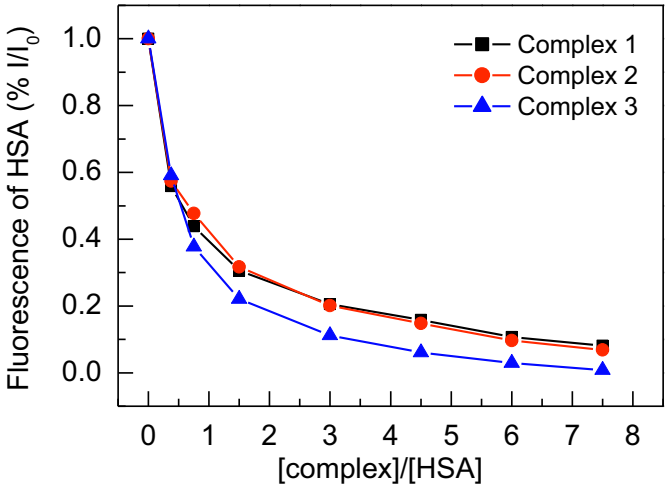

Fig. 18. Dependence of relative fluorescence intensity in % at 347 nm versus concentration ratio of complex and human serum albumin ([complex]/[HSA]) for complexes **1–3** in buffer solution. Legend: [Cu(tolf-*O*,*O*′)$_2$(phen)] (**1**); [Cu(mef-*O*,*O*′)$_2$(phen)] (**2**); [Cu(fluf-*O*,*O*′)$_2$(phen)] (**3**).

Table 6
The values of the dynamic quenching constants (K_{sv}), quenching constants (k_q), association binding constants (*K*) and the number of binding sites per albumin (*n*) obtained for the interaction of complexes **1–3** with human serum albumin.

Complex	K_{SV} (M^{-1})	k_q ($M^{-1}\,s^{-1}$)	*K* (M^{-1})	*n*
[Cu(tolf-*O*,*O*′)$_2$(phen)] (**1**)	7.05×10^5	7.05×10^{13}	1.08×10^6	0.94
[Cu(mef-*O*,*O*′)$_2$(phen)] (**2**)	8.55×10^5	8.55×10^{13}	9.01×10^5	0.98
[Cu(fluf-*O*,*O*′)$_2$(phen)] (**3**)	2.24×10^6	2.24×10^{14}	8.22×10^5	1.07

constants (*K*) indicate that the albumin may act as a targeted drug delivery vehicle for all three complexes. However, it should be noted that these *K* values are within the optimal range, indicating that they are high enough to transport the drug, although well below the limiting values found for the tetrameric biotin-binding protein avidin ($K \sim 10^{15}\ M^{-1}$) which represents one of the strongest known types of non-covalent bonding [91]. This implies that the albumin-bound complexes can be released from the carrier, once they reach the target.

3.8. Anticancer activity of copper(II) complexes

The anticancer activities of complexes **1–3** have been investigated under identical conditions using MTS assay against three cancer cell lines: HT-29 human colon adenocarcinoma cell line, HeLa cells, T-47D breast cancer cell line and the MSC mesenchymal stromal cell line. IC_{50} values were determined for all three complexes (Table 7), and the results clearly indicate that all three complexes are highly cytotoxic against all three cancer cell lines. The growth curves for all three cancer cell lines and mesenchymal stromal cells are presented in Fig. 19.

All three cancer cell lines revealed a similar susceptibility toward complexes **1–3**. The obtained values of IC_{50} revealed that while Hela

Table 7
IC_{50} values calculated by Calcusyn for 3 cancer cell lines and MSC incubated 4 days with complexes **1–3**. The results are from two independent experiments measured in quadruplicates. Legend: [Cu(tolf-*O*,*O*′)$_2$(phen)] (**1**); [Cu(mef-*O*,*O*′)$_2$(phen)] (**2**); [Cu(fluf-*O*,*O*′)$_2$(phen)] (**3**).

Cell line IC_{50}	Complex 1	Complex 2	Complex 3
HT-29	1.336 (r = 0.84511)	1.337 (r = 0.94026)	1.400 (r = 0.87721)
HeLa	1.739 (r = 0.86045)	1.555 (r = 0.96485)	2.437 (r = 0.96474)
T-47D	0.836 (r = 0.99782)	0.915 (r = 0.99809)	0.800 (r = 1.00000)
MSC	3.970 (r = 0.97444)	4.713 (r = 0.96085)	4.957 (r = 0.95311)

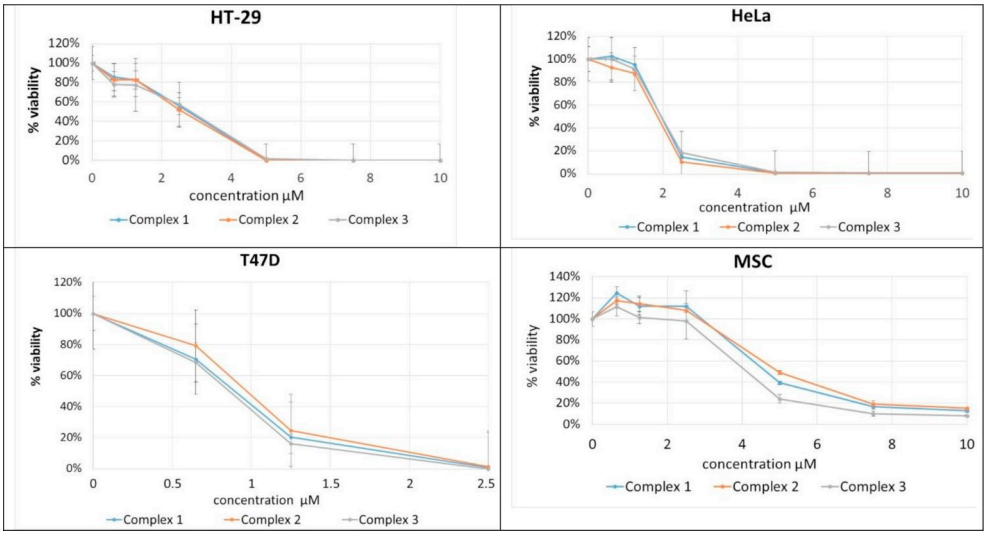

Fig. 19. Grow curves of three cancer cell lines (HT-29, HeLa and T47D) and MSC in the presence of complexes **1–3**. Tested concentrations were: 0; 0.65; 1.25; 2.5; 5; 7.5 and 10.0 μM. Legend: [Cu(tolf-*O*,*O*′)$_2$(phen)] (**1**), [Cu(mef-*O*,*O*′)$_2$(phen)] (**2**), [Cu(fluf-*O*,*O*′)$_2$(phen)] (**3**).

cells are found to be the least susceptible, T-47D breast cancer cells were those most susceptible to the effects of complex **3**. The results further indicate that the cytotoxicities of the copper complexes vary slightly according to the mode and extent of their interaction with DNA and protein. Mesenchymal cells were found to be the most resistant, which accords with a high degree of selectivity and cytotoxicity of complexes **1–3** toward cancer cells [92,93].

From a consideration of the DNA damage results obtained (see above), we may conclude that the hydrophobic forces which influence the interaction and partial intercalating interaction of the copper complexes with DNA represent a common denominator for the cytotoxicity of complexes **1–3** against cancer cells. It also can be proposed that redox cycling involving the Cu(II) complexes results in the formation of ROS (superoxide radical anions, hydroxyl radicals, singlet oxygen) which may represent an alternative cytotoxicity mechanism for the metal complexes. In addition, it can be speculated that the interaction of copper(II) complexes with intracellular antioxidants, such as glutathione, may contribute to the cytotoxicity of complexes **1–3**. Immobilization of intracellular antioxidants by metal complexes represents a new approach in modern anticancer therapy [14].

4. Conclusions

In the present work, we studied the redox-cycling and intercalating properties of novel mixed Cu(II) complexes with phenanthroline and non-steroidal anti-inflammatory drugs tolfenamic acid, [Cu(tolf-*O*,*O*′)$_2$(phen)] (**1**); mefenamic acid, [Cu(mef-*O*,*O*′)$_2$(phen)] (**2**) and flufenamic acid, [Cu(fluf-*O*,*O*′)$_2$(phen)] (**3**). Tolfenamic, mefenamic and flufenamic acids differ in the nature of their aryl substituents; hence, while tolfenamate contains a chlorine atom, mefenamate has methyl groups and flufenamate contains three fluorine atoms. Our attention has been primarily focused on molecular structural properties, SOD-mimetic activity, DNA damage, interaction with human serum albumin, and anticancer activity. The major results can be summarized as follows.

All three Cu(II) complexes **1–3** are monomeric and crystallize in a monoclinic space group C2/c, but only two of the three (complexes **1** and **2**) compounds are isostructural. Both functional ligands, the intercalator (1,10-phenanthroline) and the non-steroidal anti-inflammatory drugs NSAIDs (tolfenamic, mefanamic and flufenamic acids), are coordinated to the copper atom as bidentate chelating ligands, around which they adopt a distorted octahedral coordination geometry. As expected, the more distant halogen and methyl substituents on the NSAIDs did not affect the geometry of the Cu(II) complexes to any significant degree.

The EPR spectra of complexes **1–3** are in accord with the X-ray data. The solid state EPR spectra of these Cu(II) complexes exhibit an axial symmetry with $g_{\perp} < g_{||}$. EPR spectra measured in frozen DMSO solution exhibit well resolved parallel hyperfine splittings. Based on the similarity of the EPR data in the solid state and DMSO solution, it could be concluded that the Cu(II) complexes in DMSO solution retain similar geometry as in the solid state, which is of particular importance for drawing conclusions from biological experiments.

The similarity of the redox potential values of all three Cu(II) complexes confirms that the effect of the remote substituents (chlorine in **1**, methyl in **2** and fluorine in **3**) is minimal. The values of $E_{1/2}$ for all three complexes are within the range (−0.363 and 0.687 V vs Ag/AgCl), which is necessary for effective dismutation of the superoxide radical anion to occur, which makes them of interest as prospective SOD-mimetic compounds.

Absorption titrations have been applied to detect the mode and strength of the interaction of the Cu(II) complexes with the DNA molecule. The obtained values of the binding constants (K_b) are of the order of $\sim 10^5\,M^{-1}$. This is considered to be an indication that the interaction is relatively strong, and in the order **3** > **2**~**1**.

The binding mode of Cu(II) complexes with DNA was further studied by means of viscosity measurements. Addition of the complexes **1–3** to a solution containing DNA resulted in a significant increase in the relative viscosity and we may deduce that the intercalation ability of complexes is in the order **3** > **2** > **1**, in agreement with results from the absorption titrations. In contrast to the molecular planes of the complexes **1** and **2**, that in flufenamic acid (complex **3**, which contains three fluorine atoms), is oriented in the direction of intercalation to the DNA. In line with this, the fact that the greatest intercalating ability is found for complex **3** can be explained by the formation of weak hydrogen bonds between the electron pairs of three fluorine atoms and hydrogen atoms at the surface of DNA. Accordingly, it can be proposed that remote substituents are able to effectively modulate the strength of intercalation of the metal complexes into DNA.

The nuclease activity of the Cu(II) complexes and the mechanism of their damage to DNA were studied using gel electrophoresis. The obtained results revealed the ability of complexes **1–3** to cleave DNA (even in the absence of hydrogen peroxide) in the order **3** > **2** > **1**, in agreement with both the viscosity measurements and the absorption titrations. Under the conditions of a simulated Fenton reaction (formation of hydroxyl radicals in the presence of hydrogen peroxide), the

activities of the complexes are also in the order **3** > **2** > **1**, and hence we conclude that in addition to intercalation, the formation of ROS provides an additional mechanism for DNA damage. Application of the ROS scavengers, L-histidine, DMSO, and SOD, confirmed, respectively, the formation of singlet oxygen, hydroxyl radicals, and superoxide radical anions. Hence, we may deduce that both the intercalation mechanism, and the deleterious effect of ROS are involved in DNA damage.

The studied Cu(II) complexes exhibit an excellent SOD-mimetic activity toward the dismutation of superoxide radical anion (IC_{50} values ranging from 0.94 to 1.23 μM) and this activity was found to decrease in the order **3–1** > **2**. In agreement with the electrochemical measurements, we propose that the interaction of superoxide radical anion with the Cu(II) moiety in these complexes gives rise to redox cycling reactions (Eqs. (9)–(11)):

$$Cu(II) - L + O_2^{\bullet -} - \rightarrow Cu(I) - L + O_2 \quad (9)$$

$$Cu(I) - L + O_2^{\bullet -} + 2H^+ \rightarrow Cu(II) - L + H_2O_2 \quad (10)$$

$$Cu(I) - L + H_2O_2 \rightarrow Cu(II) - L + {}^{\bullet}OH + OH^- \text{ (Fenton reaction)} \quad (11)$$

Reduction of Cu(II) to Cu(I), following interaction of the Cu(II) complexes with superoxide radical anions has been evidenced by the application of specific chelator of Cu(I) species neocuproine and using EPR spectroscopy.

Fluorescence spectroscopy measurements revealed that all three complexes interact with human serum albumin. Since the values determined for the association binding constants between Cu(II) complexes and HSA are relatively high ($K \sim 10^6$), the possibility is offered that the albumin may act as a targeted drug delivery vehicle for all three complexes.

The anticancer activities of complexes **1–3** have been investigated using an MTS assay against three cancer cell lines: HT-29 human colon adenocarcinoma cell line, HeLa cells, T-47D breast cancer cell line and mesenchymal stromal cell (MSC) line. All three cancer cell lines revealed a similar susceptibility toward the complexes. Conversely, mesenchymal cells proved to be the most resistant, which indicates that there is a high degree of selectivity and cytotoxicity of the complexes **1–3** in their action against cancer cells.

From all of the above, we may conclude that Cu(II) complexes **1–3** are both excellent SOD-mimetic compounds and efficient DNA intercalators. In addition, their action in promoting DNA damage is a result of a redox-cycling mechanism, which causes the formation of singlet oxygen, hydroxyl radicals and superoxide radical anions. Cu(II) complexes interact with human serum albumin which may provide a vehicle for targeted drug delivery. From an anticancer study it was confirmed, that HT-29 human colon adenocarcinoma cell line, HeLa cells, and T-47D breast cancer cell line are susceptible to the action of all three complexes. In contrast, the resistance of mesenchymal cells against the Cu(II) complexes confirmed that these compounds exhibit a high degree of selectivity and cytotoxicity. However, the most promising compound from the viewpoint of its biological activity is complex **3**, with fluorine atoms present on the NSAID moiety.

The overall results indicate that a conformational change occurs in the DNA, which then undergoes cleavage, and that its ability to bind to proteins are requisite features for the Cu(II) complexes to act as anticancer agents. Further mechanistic investigations are necessary to fully understand the detailed molecular mechanism of cytotoxicity of Cu(II) complexes and hence to verify our hypothesis.

Acknowledgements

This work was supported by Scientific Grant Agency (VEGA Projects 1/0686/17, 1/0489/16, 1/0639/18), Research and Development Support Agency (APVV-15-0079).

Appendix A. Supplementary data

Supplementary data to this article can be found online at https://doi.org/10.1016/j.jinorgbio.2019.02.010.

References

[1] N. Muhammad, Z. Guo, Curr. Opin. Chem. Biol. 19 (2014) 144–153.
[2] U. Ndagi, N. Mhlongo, M.E. Soliman, Drug Des. Devel. Ther. 11 (2017) 599–616.
[3] J. Deng, P. Yu, Z. Zhang, J. Wang, J. Cai, N. Wu, H. Sun, H. Liang, F. Yang, Eur. J. Med. Chem. 158 (2018) 442–452.
[4] Q. Mo, J. Deng, Y. Liu, G. Huang, Z. Li, P. Yu, Y. Gou, F. Yang, Eur. J. Med. Chem. 156 (2018) 368–380.
[5] Z.F. Chen, C. Orvig, H. Liang, Curr. Top. Med. Chem. 17 (2017) 3131–3145.
[6] J. Qi, Q. Yao, L. Tian, Y. Wang, Eur. J. Med. Chem. 158 (2018) 853–862.
[7] M. Pal, U. Nandi, D. Mukherjee, Eur. J. Med. Chem. 150 (2018) 419–445.
[8] K.M. Deo, B.J. Pages, D.L. Ang, C.P. Gordon, J.R. Aldrich-Wright, Int. J. Mol. Sci. 17 (2016) 1818.
[9] E.C. Long, J.K. Barton, Acc. Chem. Res. 23 (1990) 271–273.
[10] B.M. Zeglis, V.C. Pierre, J.K. Barton, Chem. Commun. (Camb). (2007) 4565–4579.
[11] H.K. Liu, P.J. Sadler, Acc. Chem. Res. 44 (2011) 349–359.
[12] U. Jungwirth, C.R. Kowol, B.K. Keppler, C.G. Hartinger, W. Berger, P. Heffeter, Antioxid. Redox Signal. 15 (2011) 1085–1127.
[13] A. Zafar, S. Singh, I. Naseem, J. Nutr. Biochem. 33 (2016) 15–27.
[14] P. Poprac, K. Jomova, M. Simunkova, V. Kollar, C.J. Rhodes, M. Valko, Trends Pharmacol. Sci. 38 (2017) 592–607.
[15] J.R. Sorenson, G.W. Wangila, Curr. Med. Chem. 14 (2007) 1499–1503.
[16] J.R. Sorenson, J. Med. Chem. 27 (1984) 1747–1749.
[17] Y.Y. Qi, Q. Gan, Y.X. Liu, Y.H. Xiong, Z.W. Mao, X.Y. Le, Eur. J. Med. Chem. 154 (2018) 220–232.
[18] J. Gazo, I.B. Bersuker, J. Garaj, M. Kabesova, J. Kohout, H. Langfelderova, M. Melnik, M. Serator, F. Valach, Coord. Chem. Rev. 19 (1976) 253–297.
[19] J.E. Weder, C.T. Dillon, T.W. Hambley, B.J. Kennedy, P.A. Lay, J.R. Biffin, H.L. Regtop, N.M. Davies, Coord. Chem. Rev. 232 (2002) 95–126.
[20] C. Tolia, A.N. Papadopoulos, C.P. Raptopoulou, V. Psycharis, C. Garino, L. Salassa, G. Psomas, J. Inorg. Biochem. 123 (2013) 53–65.
[21] A. Tarushi, S. Perontsis, A.G. Hatzidimitriou, A.N. Papadopoulos, D.P. Kessissoglou, G. Psomas, J. Inorg. Biochem. 149 (2015) 68–79.
[22] F. Dimiza, S. Fountoulaki, A.N. Papadopoulos, C.A. Kontogiorgis, V. Tangoulis, C.P. Raptopoulou, V. Psycharis, A. Terzis, D.P. Kessissoglou, G. Psomas, Dalton Trans. 40 (2011) 8555–8568.
[23] S. Perontsis, A.G. Hatzidimitriou, O.A. Begou, A.N. Papadopoulos, G. Psomas, J. Inorg. Biochem. 162 (2016) 22–30.
[24] S. Fountoulaki, F. Perdih, I. Turel, D.P. Kessissoglou, G. Psomas, J. Inorg. Biochem. 105 (2011) 1645–1655.
[25] F. Dimiza, F. Perdih, V. Tangoulis, I. Turel, D.P. Kessissoglou, G. Psomas, J. Inorg. Biochem. 105 (2011) 476–489.
[26] M. Valko, D. Leibfritz, J. Moncol, M.T. Cronin, M. Mazur, J. Telser, Int. J. Biochem. Cell Biol. 39 (2007) 44–84.
[27] A.L. Abuhijleh, J. Khalaf, Eur. J. Med. Chem. 45 (2010) 3811–3817.
[28] E. Grueso, G. Lopez-Perez, M. Castellano, R. Prado-Gotor, J. Inorg. Biochem. 106 (2012) 1–9.
[29] E. Tselepi-Kalouli, N. Katsaros, J. Inorg. Biochem. 37 (1989) 271–282.
[30] M.C. Burla, R. Caliandro, M. Camalli, B. Carrozzini, G.I. Cascarano, C. Giacovazzo, M. Mallamo, A. Mazzone, G. Polidori, R. Spagna, J. Appl. Crystallogr. 45 (2012) 357–361.
[31] L. Palatinus, G. Chapuis, J. Appl. Crystallogr. 40 (2007) 786–790.
[32] G.M. Sheldrick, Acta Crystallogr., Sect. C 71 (2015) 3–8.
[33] O.V. Dolomanov, L.J. Bourhis, R.J. Gildea, J.A.K. Howard, H. Puschmann, J. Appl. Crystallogr. 42 (2009) 339–341.
[34] C.F. Macrae, I.J. Bruno, J.A. Chisholm, P.R. Edgington, P. McCabe, E. Pidcock, L. Rodriguez-Monge, R. Taylor, J. van de Streek, P.A. Wood, J. Appl. Crystallogr. 41 (2008) 466–470.
[35] M.J. Turner, J.J. MacKinnon, S.K. Wolff, D.J. Grimwood, P.R. Spackman, D. Jayatilaka, M.A. Spackman, Crystal Explorer17.5. University of Western Australia, Perth, 2017.
[36] F.L. Hirshfeld, Theor. Chim. Acta 44 (1977) 129–138.
[37] M.A. Spackman, D. Jayalitaka, Cryst. Eng. Comm. 11 (2009) 19–32.
[38] M.A. Spackman, J.J. McKinnon, Cryst. Eng. Comm. 4 (2002) 378–392.
[39] A. Parkin, G. Barr, W. Dong, C.J. Gilmore, D. Jayalitaka, J.J. McKinnon, M.A. Spackman, C.C. Wilson, Cryst. Eng. Comm. 9 (2007) 648–652.
[40] A. Wolfe, G.H. Shimer Jr., T. Meehan, Biochemistry 26 (1987) 6392–6396.
[41] A.M. Pyle, J.P. Rehmann, R. Meshoyrer, C.V. Kumar, N.J. Turro, J.K. Barton, J. Am. Chem. Soc. 111 (1989) 3051–3058.
[42] G. Czapski, A. Samuni, S. Goldstein, Methods Enzymol. 349 (2002) 234–242.
[43] D. Kovala-Demertzi, A. Galani, M.A. Demertzis, S. Skoulika, C. Kotoglou, J. Inorg. Biochem. 98 (2004) 358–364.
[44] J.R. Lakowicz, G. Weber, Biochemistry 12 (1973) 4161–4170.
[45] S. Wu, W. Yuan, H. Wang, Q. Zhang, M. Liu, K. Yu, J. Inorg. Biochem. 102 (2008) 2026–2034.
[46] L. Kucerova, V. Altanerova, M. Matuskova, S. Tyciakova, C. Altaner, Cancer Res. 67 (2007) 6304–6313.
[47] J.J. McKinnon, M.A. Spackman, A.S. Mitchell, Acta Crystallogr. B 60 (2004) 627–668.

[48] J.J. McKinnon, D. Jayatilaka, M.A. Spackman, Chem. Commun. (2007) 3814–3816.
[49] R. Klement, F. Stock, H. Elias, H. Paulus, P. Pelikan, M. Valko, M. Mazur, Polyhedron 18 (1999) 3617–3628.
[50] A. Abragam, B. Bleaney, Electron Paramagnetic Resonance of Transition Ions, Clarendon Press, Oxford, 1970.
[51] J. Kohout, M. Hvastijova, J. Kozisek, J.G. Diaz, M. Valko, L. Jager, I. Svoboda, Inorg. Chim. Acta 287 (1999) 186–192.
[52] J. Svorec, M. Valko, J. Moncol, M. Mazur, M. Melnik, J. Telser, Transit. Met. Chem. 34 (2008) 129–134.
[53] M. Valko, M. Melnik, P. Pelikan, F. Valach, M. Mazur, Chem. Phys. Lett. 174 (1990) 591–594.
[54] G. Valora, R.P. Bonomo, G. Tabbi, Inorg. Chim. Acta 453 (2016) 62–68.
[55] M. Valko, H. Morris, M. Mazur, J. Telser, E.J.L. McInnes, F.E. Mabbs, J. Phys. Chem. B 103 (1999) 5591–5597.
[56] U. Sakaguschi, A.W. Addion, J. Chem. Soc. Dalton Trans. (1979) 600–608.
[57] M. Puchonova, S. Matejova, V. Jorik, I. Salitros, L. Svorc, M. Mazur, J. Moncol, D. Valigura, Polyhedron 151 (2018) 152–159.
[58] P.M. Takahara, A.C. Rosenzweig, C.A. Frederick, S.J. Lippard, Nature 377 (1995) 649–652.
[59] A.C. Komor, J.K. Barton, Chem. Commun. 49 (2013) 3617–3630.
[60] M. Sirajuddin, S. Ali, A. Badshah, J. Photochem. Photobiol. B Biol. 124 (2013) 1–9.
[61] S. Tsiliou, L.A. Kefala, F. Perdih, I. Turel, D.P. Kessissoglou, G. Psomas, Eur. J. Med. Chem. 48 (2012) 132–142.
[62] R.S. Kumar, S. Arunachalam, Eur. J. Med. Chem. 44 (2009) 1878–1883.
[63] L. Wang, Y. Wu, T. Chen, C. Wei, Int. J. Biol. Macromol. 52 (2013) 1–8.
[64] P. Pakravan, S. Kashanian, M.M. Khodaei, F.J. Harding, Pharmacol. Rep. 65 (2013) 313–335.
[65] T. Topala, A. Bodoki, L. Oprean, R. Oprean, Farmacia 62 (2014) 1049–1061.
[66] S.U. Rehman, Z. Yaseen, M.A. Husain, T. Sarwar, H.M. Ishqi, M. Tabish, PLoS One 9 (2014) e93913.
[67] J. Liu, T. Zhang, T. Lu, L. Qu, H. Zhou, Q. Zhang, L. Ji, J. Inorg. Biochem. 91 (2002) 269–276.
[68] S. Sobha, R. Mahalakshmi, N. Raman, Spectrochim. Acta A 92 (2012) 175–183.
[69] M.N. Patel, P.A. Dosia, B.S. Bhatt, V.R. Thakkar, Spectrochim. Acta A 78 (2011) 763–770.
[70] G. Yang, J.A. Wu, L. Wang, L.N. Ji, X. Tian, J. Inorg. Biochem. 66 (1997) 141–144.
[71] F. Dimiza, F. Perdih, V. Tangoulis, J. Inorg. Biochem. 105 (2011) 476–489.
[72] E. Chalkidou, F. Perdih, I. Turel, J. Inorg. Biochem. 113 (2012) 55–65.
[73] S. Banerjee, S. Mondal, W. Chakraborty, S. Sen, R. Gachhui, R.J. Butcher, A.M.Z. Slawin, C. Mandal, S. Mitra, Polyhedron 28 (2009) 2785–2793.
[74] S.R. Chowdhury, S. Chatterjee, S. Igarashi, Y. Yukawa, K.K. Mukherjea, J. Coord. Chem. 65 (2012) 3469–3480.
[75] F. Arjmand, A. Jamsheera, M. Afzal, S. Tabassum, Chirality 24 (2012) 977–986.
[76] B.C. Baguley, E.M. Falkenhaug, Nucleic Acids Res. 5 (1978) 161–171.
[77] C. Dalvit, C. Invernizzi, A. Vulpetti, Chem. Eur. J. 20 (2014) 11058–11068.
[78] D.S. Sigman, A. Mazumder, D.M. Perrin, Chem. Rev. 93 (1993) 2295–2316.
[79] A. Rivero-Műller, Chem. Biol. Interact. 65 (2007) 189–199.
[80] S. Tardito, L. Marchiò, Curr. Med. Chem. 16 (2009) 1325–1348.
[81] B.C. Bales, T. Kodama, Y.N. Weledji, M. Pitié, B. Meunier, M.M. Greenberg, Nucleic Acids Res. 33 (2005) 5371–5379.
[82] A.R. Chakravarty, P.A.N. Reddy, B.K. Santra, A.M. Thomas, J. Chem. Sci. 114 (2002) 391–401.
[83] A. Kellett, O. Howe, M. O'Connor, B.S. McCann, S. Creaven, A. McClean, A. Foltyn-Arfa, M. Devereux Casey, Free Radic. Biol. Med. 53 (2012) 564–576.
[84] M. O'Connor, A. Kellett, M. McCann, G. Rosair, M. McNamara, O. Howe, B.S. Creaven, S. McClean, A.F. Kia, D. O'Shea, M. Devereux, J. Med. Chem. 55 (2012) 1957–1968.
[85] J. Prousek, Pure Appl. Chem. 79 (2007) 2325–2338.
[86] U. Weser, K.H. Sellinger, E. Lengfelder, W. Werner, J. Strahle, Biochim. Biophys. Acta 631 (1980) 232–245.
[87] A. Latif-Abuhijleh, J. Khalaf, Eur. J. Med. Chem. 45 (2010) 3811–3817.
[88] J.E. Weder, C.T. Dillon, T.W. Hambley, Coord. Chem. Rev. 232 (2002) 95–126.
[89] V. Brezova, M. Valko, M. Breza, H. Morris, J. Telser, D. Dvoranova, K. Kaiserova, L. Varecka, M. Mazur, D. Leibfritz, J. Phys. Chem. B 107 (2003) 2415–2425.
[90] Y.-Q. Wang, H.-M. Zhang, G.-C. Zhang, W.-H. Tao, S.-H. Tang, J. Lumin. 126 (2007) 211–218.
[91] V. Rajendiran, R. Karthik, M. Palaniandavar, H. Stoeckli-Evans, V.S. Periasamy, M.A. Akbarsha, B.S. Srinag, H. Krishnamurthy, Inorg. Chem. 46 (2007) 8208–8221.
[92] J. Li, H.K. Law, Y.L. Lau, G.C. Chan, Br. J. Haematol. 127 (2004) 326–334.
[93] W. Liang, H. Xia, J. Li, R.C. Zhao, Cytotechnology 63 (2011) 523–530.